

Review

Emerging Developments on Nanocellulose as Liquid Crystals: A Biomimetic Approach

Theivasanthi Thiruganasambanthan ¹, Rushdan Ahmad Ilyas ^{2,3,*} , Mohd Nor Faiz Norrahim ^{4,*} , Thiagamani Senthil Muthu Kumar ^{5,6} , Suchart Siengchin ^{6,7} , Muhammad Syukri Mohamad Misenan ⁸ , Mohammed Abdillah Ahmad Farid ⁹, Norizan Mohd Nurazzi ¹⁰ , Muhammad Rizal Muhammad Asyraf ¹¹ , Sharifah Zarina Syed Zakaria ^{12,*} and Muhammad Rizal Razman ¹³ 

- ¹ International Research Center, Kalasalingam Academy of Research and Education, Anand Nagar, Krishnan Koil 626126, India; t.theivasanthi@klu.ac.in
 - ² School of Chemical and Energy Engineering, Faculty of Engineering, Universiti Teknologi Malaysia, Johor Bahru 81310, Malaysia
 - ³ Centre for Advanced Composite Materials (CACM), Universiti Teknologi Malaysia, Johor Bahru 81310, Malaysia
 - ⁴ Research Centre for Chemical Defence, Universiti Pertahanan Nasional Malaysia, Kem Perdana Sungai Besi, Kuala Lumpur 57000, Malaysia
 - ⁵ Department of Mechanical Engineering, Kalasalingam Academy of Research and Education, Anand Nagar, Krishnan Koil 626126, India; tsmkumar@klu.ac.in
 - ⁶ Department of Materials and Production Engineering, The Sirindhorn International Thai-German Graduate School of Engineering (TGGS), King Mongkut's University of Technology North Bangkok, 1518 Wongsawang Road, Bangsue, Bangkok 10800, Thailand; suchart.s.pe@tggs-bangkok.org
 - ⁷ Institute of Plant and Wood Chemistry, Technische Universität Dresden, Piennner Str. 19, 01737 Tharandt, Germany
 - ⁸ Department of Chemistry, College of Arts and Science, Yildiz Technical University, Davutpasa Campus, Istanbul 34220, Turkey; syukrimisenan@gmail.com
 - ⁹ Department of Bioprocess Technology, Faculty of Biotechnology and Biomolecular Sciences, Universiti Putra Malaysia, Serdang 43400, Malaysia; abdillah.upm@gmail.com
 - ¹⁰ Center for Defence Foundation Studies, Universiti Pertahanan Nasional Malaysia, Kem Perdana Sungai Besi, Kuala Lumpur 57000, Malaysia; mohd.nurazzi@gmail.com
 - ¹¹ Institute of Energy Infrastructure, Universiti Tenaga Nasional, Jalan IKRAM-UNITEN, Kajang 43000, Malaysia; asyraf96@gmail.com
 - ¹² Research Centre for Environment, Economic and Social Sustainability (KASES), Institute for Environment and Development (LESTARI), Universiti Kebangsaan Malaysia (UKM), Bangi 43600, Malaysia
 - ¹³ Research Centre for Sustainability Science and Governance (SGK), Institute for Environment and Development (LESTARI), Universiti Kebangsaan Malaysia (UKM), Bangi 43600, Malaysia; mrizal@ukm.edu.my
- * Correspondence: ahmadilyas@utm.my (R.A.I.); faiznorrahim@gmail.com (M.N.F.N.); szarina@ukm.edu.my (S.Z.S.Z.)



Citation: Thiruganasambanthan, T.; Ilyas, R.A.; Norrahim, M.N.F.; Kumar, T.S.M.; Siengchin, S.; Misenan, M.S.M.; Farid, M.A.A.; Nurazzi, N.M.; Asyraf, M.R.M.; Zakaria, S.Z.S.; et al. Emerging Developments on Nanocellulose as Liquid Crystals: A Biomimetic Approach. *Polymers* **2022**, *14*, 1546. <https://doi.org/10.3390/polym14081546>

Academic Editor: Luis Alves

Received: 21 February 2022

Accepted: 14 March 2022

Published: 11 April 2022

Publisher's Note: MDPI stays neutral with regard to jurisdictional claims in published maps and institutional affiliations.



Copyright: © 2022 by the authors. Licensee MDPI, Basel, Switzerland. This article is an open access article distributed under the terms and conditions of the Creative Commons Attribution (CC BY) license (<https://creativecommons.org/licenses/by/4.0/>).

Abstract: Biomimetics is the field of obtaining ideas from nature that can be applied in science, engineering, and medicine. The usefulness of cellulose nanocrystals (CNC) and their excellent characteristics in biomimetic applications are exciting and promising areas of present and future research. CNCs are bio-based nanostructured material that can be isolated from several natural biomasses. The CNCs are one-dimensional with a high aspect ratio. They possess high crystalline order and high chirality when they are allowed to assemble in concentrated dispersions. Recent studies have demonstrated that CNCs possess remarkable optical and chemical properties that can be used to fabricate liquid crystals. Research is present in the early stage to develop CNC-based solvent-free liquid crystals that behave like both crystalline solids and liquids and exhibit the phenomenon of birefringence in anisotropic media. All these characteristics are beneficial for several biomimetic applications. Moreover, the films of CNC show the property of iridescent colors, making it suitable for photonic applications in various devices, such as electro-optical devices and flat panel displays.

Keywords: nanocellulose; cellulose nanocrystals; liquid crystals; biomimetic

1. Introduction

Liquid crystals denote an intermediate condition between crystalline solid and amorphous liquid, making it a mesophase. Like a liquid, they have some degree of isotropy. Simultaneously, a crystal's order can be preserved in at least one direction, resulting in anisotropic molecules with no positional order and just orientational order [1]. The characteristic of rod-like liquid arrangement during the crystalline phase with liquid and crystalline solid is depicted in Figure 1. The liquid crystalline phase structure can be found in a variety of living organisms, including plants, animals, and microorganisms. For instance, cellular membranes are made up of a lyotropic liquid crystalline phase that forms when phospholipids dissolve in water. The curvature of the membrane is essential for its function, particularly in cell signaling and trafficking, as well as the mycobacterial lipids release [2].

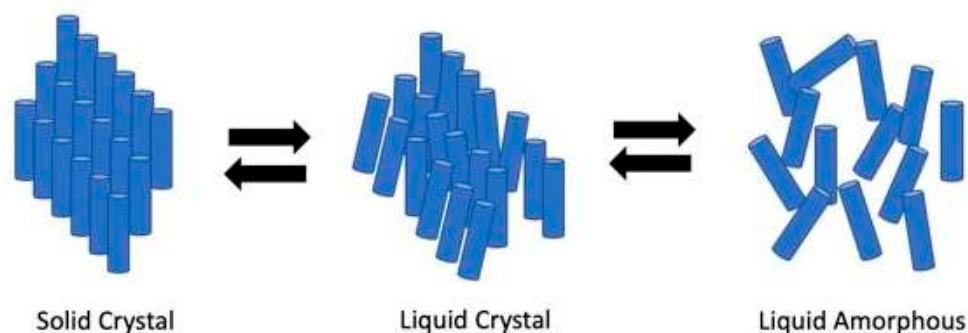


Figure 1. Illustration of rod-like particles of solid crystal, liquid crystals, and liquid phase.

Inspired by nature, the development of novel biomimetic functional systems that mimic both structural and adaptive properties of animals and living beings have received a lot of attention [3–7]. The bionic materials, biomimetic, or biomimicry are intended to mimic or replace the spatial and natural temporal presentations of physiological and biochemical components to restore or enhance biological functioning. The modeling of one or more biological systems' functional principles is all that is required for biomimetic material design. One method for developing biomimetic concepts is to list the desired system's fundamental activities first and then find a biological system that may serve as a model and execute comparable functions [8]. In regenerative medicine and regulated or target-specific drug delivery systems, rationally developed materials that investigate specific, customizable, biodegradable, and reversible interactions have benefits over non-modified standard materials. These materials are referred to as biomimetic when they are designed for detection and responding to physiological inputs or to mimic structural and functional elements of biological signals [9].

Nanomaterials derived from renewable resources are generating a lot of interest, both in fundamental science and building new structural and functional macroscopic materials [10–22]. The exceptional mechanical properties and/or photonic crystal features of biological composites, e.g., nacre, bone, beetle scales, wood, and butterfly wings, are also essential inspirations for developing novel multifunctional materials using nature-based nanomaterials. Nonetheless, to fully exploit the intrinsic features of nanosized starting materials, strong and adaptable synthetic and processing strategies to regulate assembly over many length scales must be developed [23].

For millennia, humans have been using cellulose, among nature's most versatile and broadly distributed biopolymers, as a building material, source of energy, clothing component, and a means of storing and transmitting culture and knowledge [24,25]. Presently, cellulose products are used in a wide array of uses, and the pulp and paper industry contributes significantly to the economic output of many countries [26–34]. Cellulose is insoluble in water and possesses a hydrophilic surface. Cellulose contains both amorphous and crystalline regions [35]. Oxidation of cellulose may result in carboxylic acids from some hydroxyl groups conversion [36]. Nanocellulose is spindle-shaped with Young's modulus

of more than 140 GPa. Cellulose extraction can be achieved in various sizes, depending on the desired applications [33,37,38].

In industrial practices, nanocellulose is the most frequently used cellulose size. Nanocellulose is categorized into three classes: (1) nanofibrillated cellulose (NFC) or nanofibrils or microfibrillated cellulose or microfibrils, (2) cellulose nanocrystals (CNC) or crystallites or rod-like cellulose microcrystals or whiskers, and (3) bacterial nanocellulose (BNC) or bio-cellulose or microbial cellulose [39–45]. CNC is prepared via cellulose acid hydrolysis containing natural materials like cotton and wood [46–48]. According to Kusmono et al. [49], sulfuric acid has been recognized as the acid most commonly used in hydrolysis for preparing CNC due to the process is simple and results in nanoparticles (100–1000 nm) with highly crystalline and stiff. During the acid hydrolysis process, the sulfur groups attach to the CNC surface and become negatively charged. Because of the electrostatic repulsion between the CNC particles, a good suspension is obtained. This can be analyzed by optical polarization microscopy for its liquid crystalline nature, which is suitable for more photonic applications [50].

NFC and CNC are distinguished by the distribution of wider fiber sizes in NFC and drastically shorter or narrower in CNC [51], as depicted in Figure 2. Both NFC and BNC have high crystallinity and narrow size distribution, except for BNC that is derived from bacteria. Alain Dufresne [52] and Chirayil et al. [53] reported the fame of CNC and NFC is not only due to their biodegradability, natural abundance, unique structures, superior mechanical properties, low density, high surface area and aspect ratio, and biocompatibility but also for their possibility to modify their surfaces to enhance their nano-reinforcement compatibility with other polymers due to the presence of abundant hydroxyl groups. Nanocellulose-based materials, also known as a new ageless bionanomaterial, are non-toxic, recyclable, sustainable, and carbon-neutral [52]. Nanocellulose has the properties of nanoscale dimension, low density, chirality, and thermomechanical performance. Due to these attributes, nanocellulose has gained tremendous attention from scientists. In consequence, the number of patents and publications on nanocellulose over 20 years has increased significantly from 764 in 2000 to 18,418 in 2020. In addition, this increment of more than 2300% over 20 years indicates that nanocellulose has become the advanced emerging material in the 21st century.

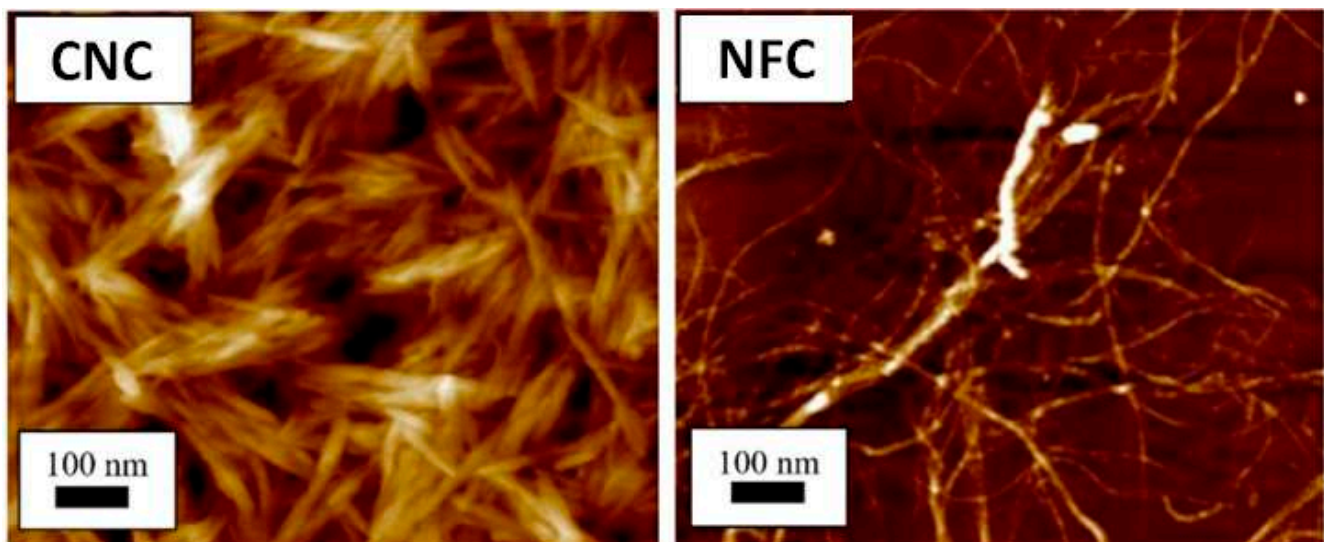


Figure 2. Atomic force microscopy images showing different structures of CNC [54] and NFC. Adapted from [55].

Assembling nanocellulose into multiphase structures leads to many advanced applications. Nanocellulose fibers contain both crystalline and amorphous phases. The OH groups' abundance on nanocellulose promotes the formation of hydrogen bonds, resulting in highly

ordered cellulose chains. They form networks when dispersed in water. Biopolymers are abundant, renewable, and sustainable [56]. By utilizing nanocellulose's colloid and interface properties, it can be formed into emulsions, solid films, foams, and aerogels. Nanocellulose self-assembly into a chiral nematic liquid crystalline phase can be applied in functional films. In concentrated dispersions, nanocellulose constructs cholesteric ordering and arranges as a chiral nematic liquid crystal. The nanocellulose films reflect the polarized light. The film color can be varied by varying the film thickness. A multilayer system can be constructed by alternate deposition of nanocellulose and a cationic polymer. Ultrasound treatment can change the chiral nematic pitch. Sonication can control the iridescent color. Externally applied electric and magnetic fields can affect the orientation. Nanopapers or nanocellulose films have good gas barrier properties since the porosity is low.

Therefore, this review aims to discuss the current research on developing nanocellulose-based solvent-free liquid crystals and their utilization in photonic applications. In addition to that, the isolation and production of CNC-based liquid crystals together with their biomimetic application were also tackled. Lastly, some future recommendations related to this study are also suggested.

2. Isolation of CNC from Several Biological Sources

In nature, cellulose exists in the form of the smallest size of an elementary fibril, regardless of the source [57,58]. There are two key steps in extracting nanoparticles from a raw cellulose sample, including (i) the source material purification and homogenization to allow homogeneous reaction conditions and (ii) the purified cellulose material separation into its components of microfibrillar and/or nanocrystalline [59].

Depending on the cellulose source, the first step is adjusted. The matrix elements removal from lignin and hemicellulose is the most critical phase for wood and plants. Luzi et al. developed a CNC extraction method from the North African grass *Ampelodesmos mauritanicus*, or Diss. The stems of the Diss were subjected to two distinct pretreatments before being extracted for nanocellulose (chemical or enzymatic). In the first pretreatment stage or the chemical pretreatment, sodium bisulfate (NaHSO_4) was employed to remove holocellulose (-cellulose + hemicellulose). The following pretreatment included the extraction of the -cellulose component and elimination of hemicellulose using sodium hydroxide (NaOH). Xylanase (Feedlyve AXC) and polygalacturonase (Peclyve EXG) enzymes were utilized in the enzymatic pretreatment. Both pretreatments aided in the reduction of fiber diameter, according to morphological analysis. New crystalline domains were created as a result of the enzymatic breakdown of cellulose, according to X-ray diffraction spectra. When compared to enzyme-treated CNC, chemically-treated CNC had lower values of mean diameter and length, as shown in Figure 3.

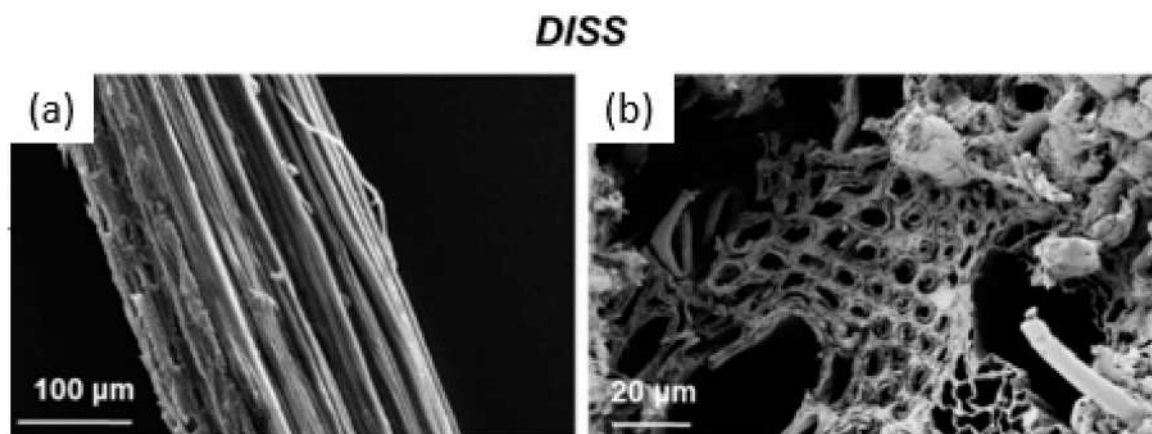


Figure 3. Cont.

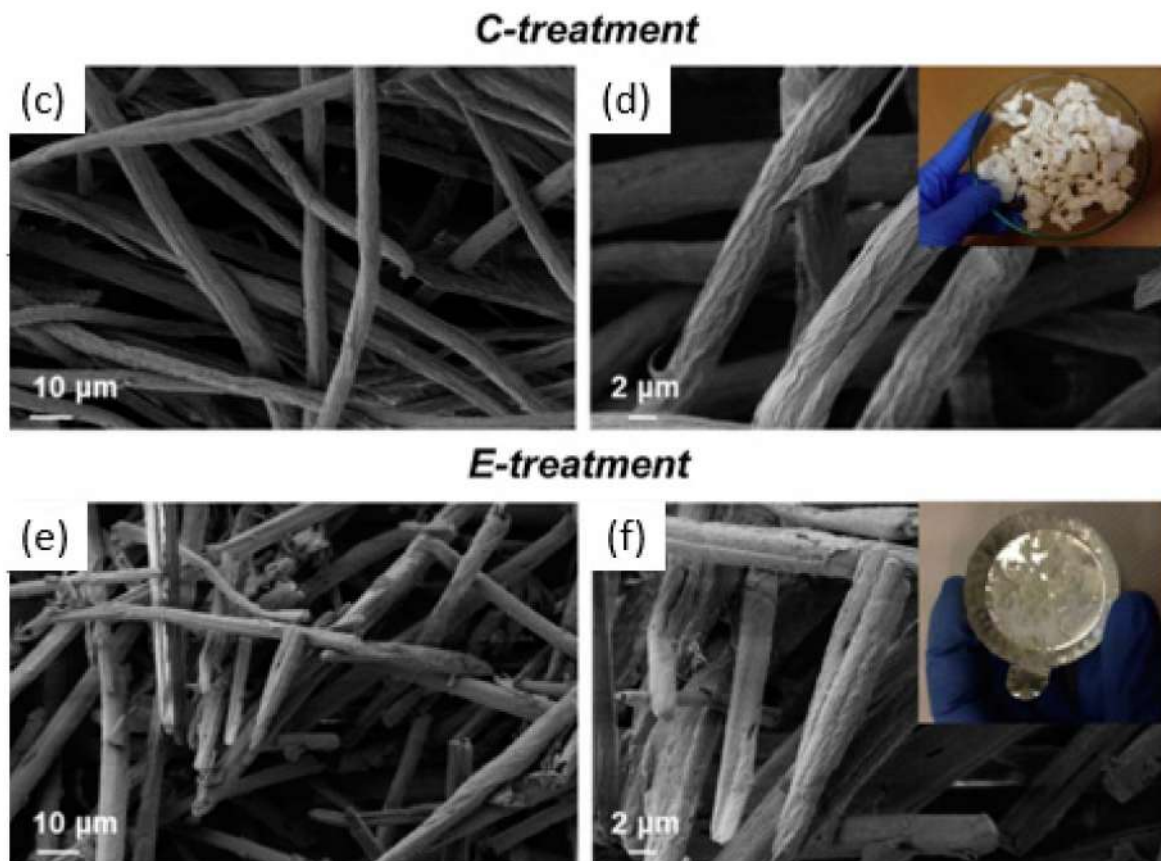


Figure 3. Morphological characterization of Diss fibers: longitudinal (a) and transversal section (b). FESEM investigation of bleached fibers using chemical (c,d) and enzymatic (e,f) treatment at two different magnifications. The visual image of treated fibers: insert (d) chemically treated fibers and insert (f) enzymatically treated fibers. Reproduced from [60].

In the second process step, acid hydrolysis, mechanical treatment, and enzymatic hydrolysis are the approaches that can be used to separate the pretreated fibers into microfibrillar or nanocrystalline components [61]. The most frequently used CNC isolation from cellulose fibers technique is acid hydrolysis, a method that dates back to Ranby's foundational studies [62], with a number of more recent modifications. The characteristics of CNC from several sources separated via sulfuric acid hydrolysis are summarized in Table 1.

Table 1. List of CNC from various cellulose sources by sulfuric acid hydrolysis.

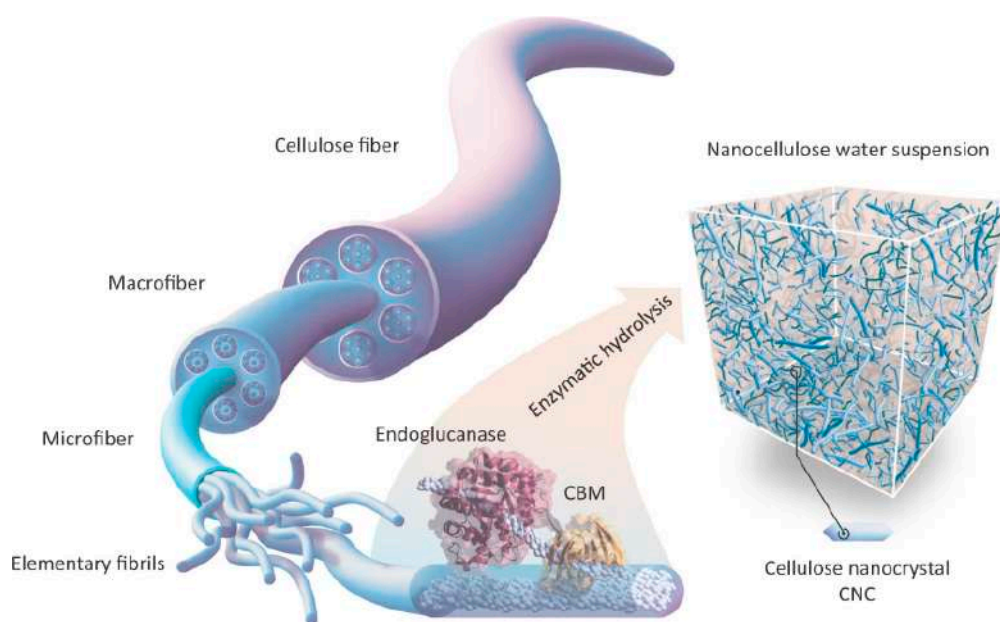
Cellulose Sources	Length (nm)	Width (nm)	Ref.
Bacteria	100–1000	10–50	[63]
Cotton	70–300	5–10	[64]
Wood	100–300	3–5	[65]
Tunicate	500–1000	10–30	[66]
Valonia	>1000	10–20	[67]

The use of enzymes in the manufacture of CNC is complicated, and they can play a variety of functions in the entire process, from eliminating pectin and hemicellulose to the most prevalent use of cellulases to form CNC. Despite the widespread belief that CNC is produced primarily through acid hydrolysis, numerous studies have shown the CNC materials production mechanisms are more varied; for example, multiple works mentioned the use of cellulases in conjunction with acid hydrolysis to produce CNC. A summary of prior research has noted the generation of CNC via enzymatic hydrolysis methods and tabulated in Table 2.

Table 2. List of previous reports regarding enzymatic hydrolysis in CNC production.

Cellulose Sources	Before Enzyme Hydrolysis	After Enzyme Hydrolysis	Enzyme	Dimensions and Crystallinity (CI)	Ref.
Sugarcane straw	Chemical treatment	-	Cellic® CTec3	D: 8.7–14.1 nm L: 395.5–507.7 nm CI: 66.7–70.4%	[68]
Eucalyptus cellulose kraft pulp	Ball milling	Sonication	On-site production by <i>A. niger</i> strain	D: 24 nm L: 294 nm CI: 77.9–78.3%	[69]
Bleached Eucalyptus kraft pulp		Sonication	Monocomponent EGs	D: 6–10 nm L: 400–600 nm CI: 88%	[70]
Sugarcane bagasse	Steam explosion/liquid hot water	Chemical treatment; acid hydrolysis	Cellic® CTec2	D: 14–18 nm L: 195–250 nm CI: 77.7%	[71]
Wheat microcrystalline cellulose	Sonication	-	Celluclast 1.5 L	D: <10 nm L: 40–200 nm CI: 74.4–87.5%	[72]

Jerma et al. [73] produced performance crystalline CNC using ancestral endoglucanase. Enzymatic hydrolysis was conducted in water at 50 °C in agitation with several endoglucanases at various times. The hierarchical structure of cellulose fiber allows for nanoscale particle destruction. They demonstrated how endoglucanase with a carbohydrate-binding module (CBM) could bind to cellulose fibers, embedding the catalytic domain in the fiber surface and increasing activity. Depending on the hydrolysis duration and enzyme used, enzyme degradation can yield nanocellulose of various sizes. The CNC is a small crystalline particle with diameters ranging from 3 to 40 nanometers and lengths ranging from 100 to 500 nanometers. Figure 4 shows the illustration of cellulose enzymatic hydrolysis.

**Figure 4.** Illustration of formation of CNC via enzyme hydrolysis. Reproduced with permission from [73].

3. Overview of CNC-Based Liquid Crystals

Revol et al. were the first to uncover the structural feature of CNC-based liquid crystals. CNC's structural property allows it to diffuse freely in water and self-organize spontaneously into a cholesteric liquid crystals phase at a low mass fraction [74]. Lower concentrations of CNC in suspension water are described to assemble isotropically (Figure 5). The suspension changed from dilute to semi dilute and concentrated isotropic assembly as the concentration rose. The CNC began to organize as tactoids above a certain concentration, which are basic phases order of liquid crystalline that forms later. During the biphasic phase, each of the liquid crystalline and isotropic order domains was in balance with the other. A higher concentration results in excellent liquid crystalline order, and the shift from the liquid crystalline to the gel state is a complex interaction of interparticle attraction and concentration. Electrolytes can compress the electrical double layers, which lessens the repulsion of charged particles and, according to reports, causes a shift between liquid and solid phases [75].

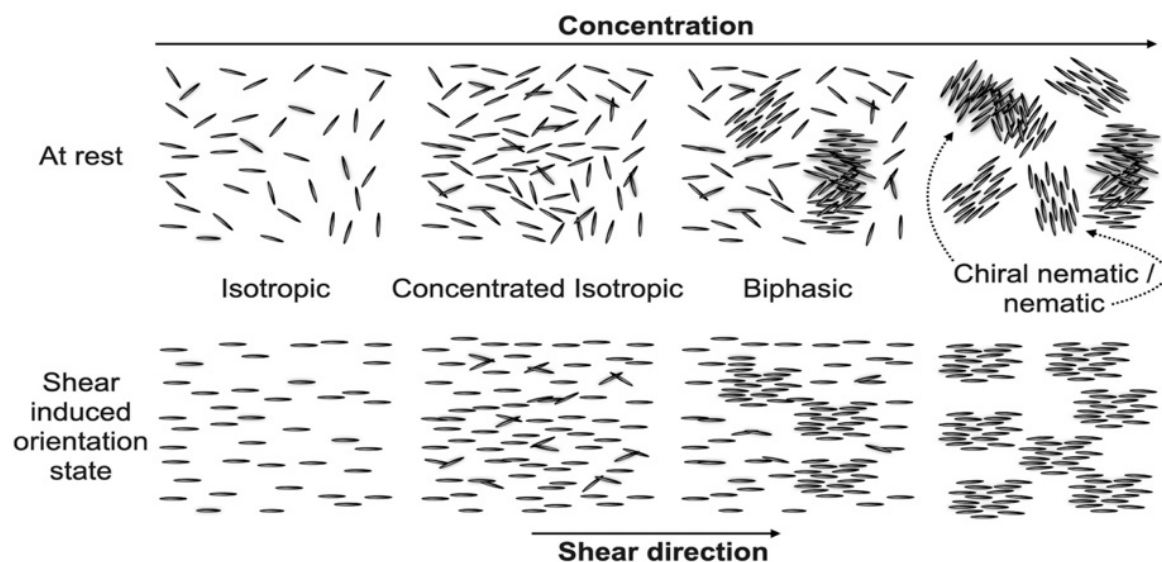


Figure 5. CNC self-assembly in a suspension at rest with rising concentration (**upper row**) and corresponding assembly in shear (**bottom row**).

On the other hand, the anisotropic structure creation within a soft solid suspension is feasible when the isotropic-nematic and liquid-solid transitions coincide. The liquid crystal re-entrance, as well as the presence of an anisotropic soft solid, resulted from research into these two competing transitions (liquid crystals hydro glass, LCH). LCH is a biphasic material composed of an appealing glass matrix and a coexisting liquid crystals phase that exhibits similar viscoelastic behavior to hydrogels while allowing colloidal rods to be reversibly oriented in the liquid crystalline phase via shear forces, e.g., their structural ordering is programmable [76]. This is depicted in Figure 6 by the isotropic/anisotropic behavior of liquid/solid phases. The existence of a reentrant liquid crystals phase at a high ionic strength satisfies the conditions for the development of LCH: spinodal breakdown (and subsequent gelation) coinciding with an anisotropic liquid crystals phase. The schemes A–D in Figure 6 illustrate the interaction between liquid crystallinity and gelation in CNC suspensions using the phase transition of a 7 wt% CNC suspension containing NaCl as an example. When salt was gradually added to a liquid crystals suspension (A), the liquid crystals' phase proportion decreased at first (B) and then increased (C). The suspension was subsequently “quenched” into the unstable thermodynamic zone (D), resulting in spinodal breakdown and segregation into the DL and DS phases, yielding a biphasic LCH. The matrix of LCHs was formed by DS, a colloid-rich phase with an appealing glass

shape that gives solid-like rheological behavior. DL is a liquid crystals phase that gives anisotropic properties to LCHs.

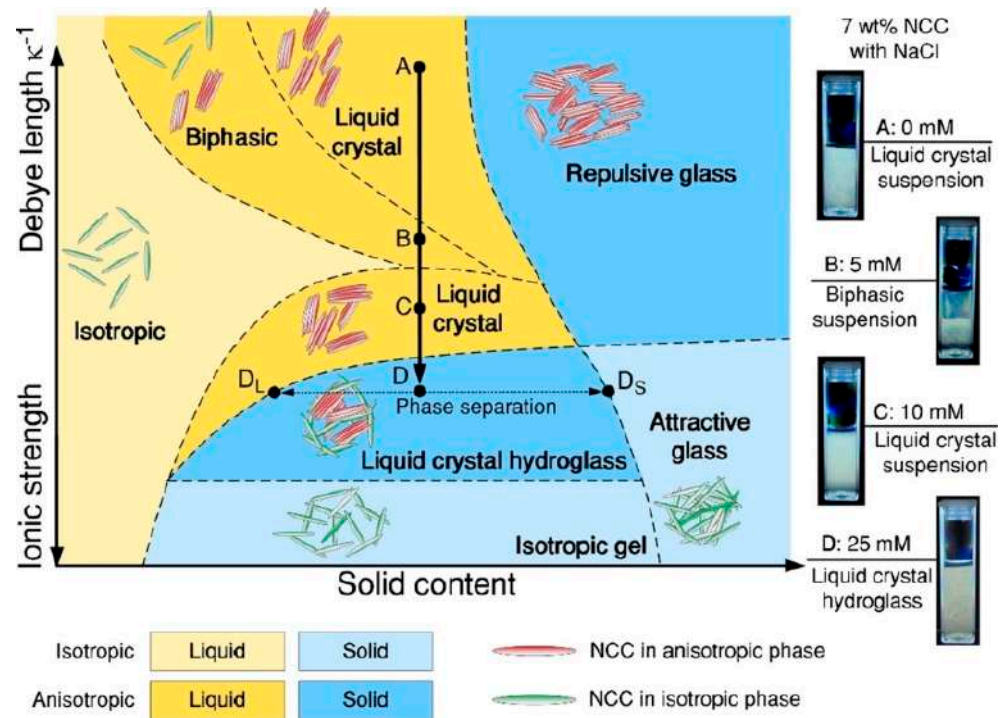


Figure 6. Schematic phase diagram of CNC aqueous suspension as a function of solid content and inter-particle attraction (represented by ionic strength). The relative positions of each phase and the geometry of the boundaries, as well as theoretical works in colloidal suspension gelation and liquid crystallinity, are from references [50,77–79]. Pictures A–D on the right were shot with cross-polarizers and corresponded to compositions A–D on the phase diagram, respectively. Reproduced from [75].

Additionally, chemically produced aqueous suspensions of CNC, avoiding electrostatic stability and encouraging steric interaction, resulted in mesophase (Figure 7) with the usual fingerprint texture [80].

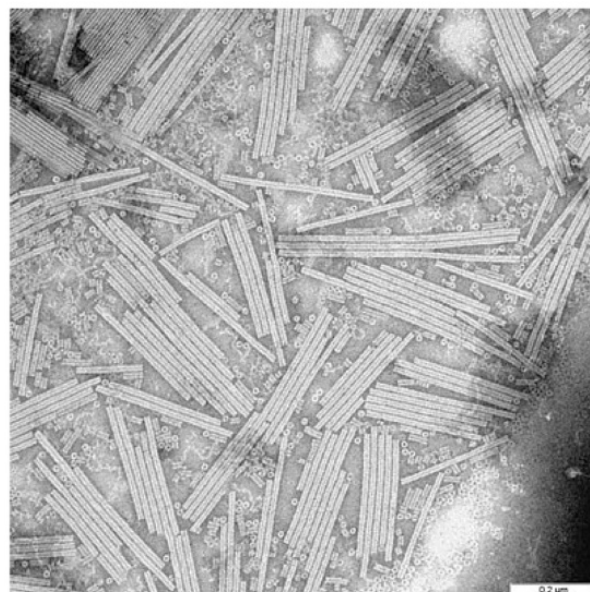


Figure 7. Cholesteric mesophase observed under electron microscopy. Reproduced from [80].

A cholesteric phase is a type of nematic phase in which the nematic phase's nanoparticle structure is chiral. One intriguing practice of the CNC solution exhibiting the cholesteric phase is the ability to dry the mixture while sustaining the chiral structure in order to produce photonic bandgap films. The chiral structure has a lot of optical activity along its helix axis. In dried CNC films, this helical structure demonstrates significant birefringence. The reflected light wavelength causing color transition is determined by the value of P , also confirmed on a CNC-based liquid crystals film. The Bragg (Vries 1951) equation describes the wavelength of reflected light, given as Equation (1):

$$\lambda = nP\sin\theta \quad (1)$$

where λ denotes the reflected wavelength, P represents the helical pitch, θ is the incident light angle ($^\circ$), $\sin\theta = 1$ when the incident light is perpendicular (90°) to the crystal plane, and n is the average refractive index of the material.

CNC aligns parallel to the director during this cholesteric phase, and its position spins through the liquid crystals along an axis perpendicular to the director, creating the helix (Figure 8a,b). De Vries devised a theory in 1951 to explain the relationship between the optical rotation and helix pitch. CNC films selectively reflect left-handed circularly polarized light due to their chiral nematic structure, resulting in a positive circular dichroism (CD) signal for transmitted light (Figure 8c,d).

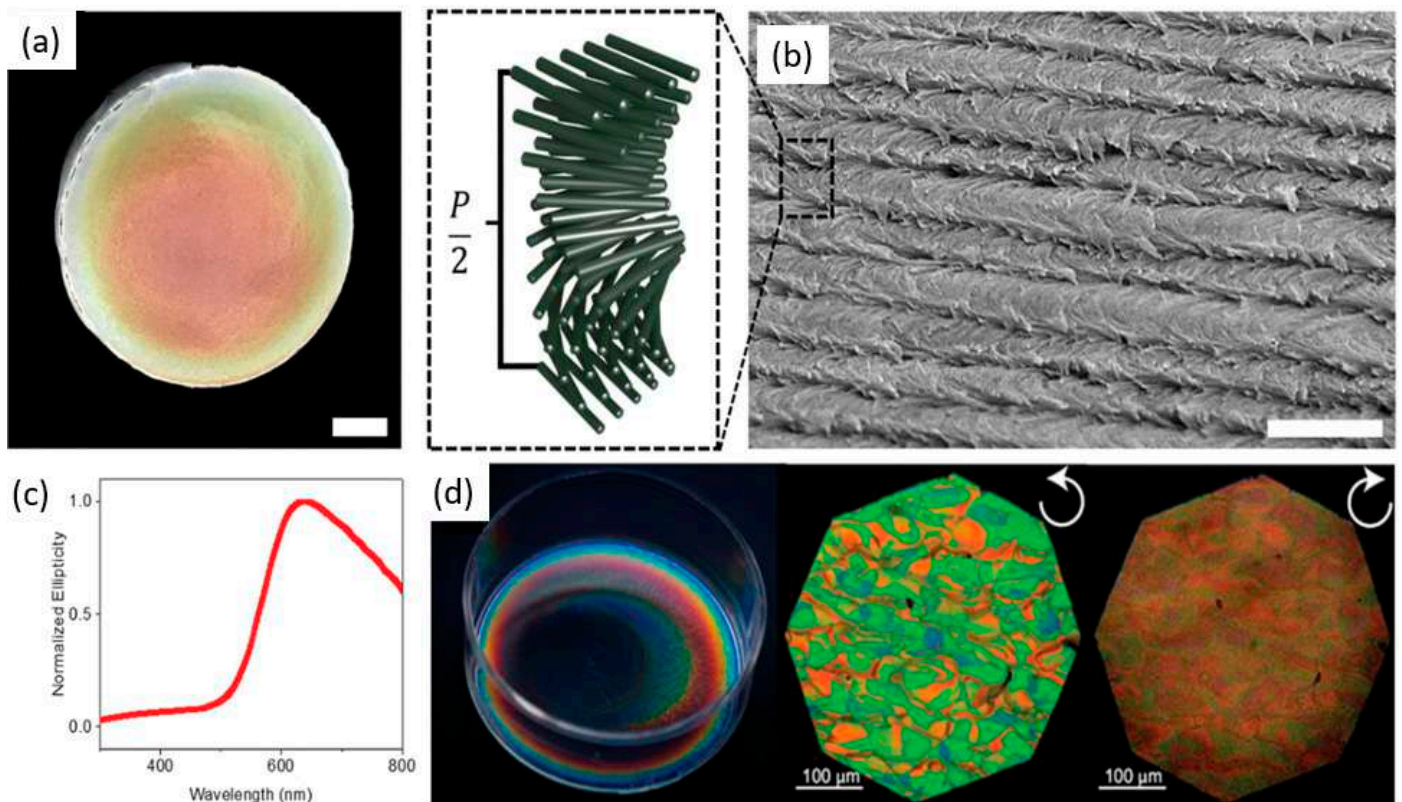


Figure 8. (a) A cholesteric CNC film's structure and optical characteristics. (b) Photograph of chiral nematic CNC film displaying structural color iridescence. (c) Scanning electron micrograph of CNC in a film with a helical twist. The helical pitch is schematically represented in the dashed-line inset (P). (d) A typical cholesteric CNC film's circular dichroism spectrum. Natural light (left), left-handed circularly polarized light (center), and right-handed circularly polarized light (right) views of chiral nematic CNC film (right). Reproduced from [81].

4. Formation Process of CNC-Based Liquid Crystals

4.1. Self-Assembly of CNC

According to Onsager's theory, the nematic ordering of rod-like CNC is determined by the balance of translational and orientational entropy. Schütz et al. reinterpreted "excluding volume" to better comprehend those entropic contributions that produced nematic ordering: the space is inaccessible for a rod due to the presence of other rods. This reduced orientational entropy and limited freedom of motion, but the total of excluded volume was limited, and translation freedom was improved by aligning themselves in a single direction, boosting translational entropy, and lowering free energy. Additionally, CNC aqueous solution can also demonstrate good stability against agglomeration due to electrostatic repulsion, which is favorable to the development of the phase of the liquid crystal.

4.1.1. Vacuum-Assisted Self-Assembly (VASA)

In 2020, Wang et al. discovered the formation of the CNC chiral nematic phase via the vacuum-assisted self-assembly (VASA) method. Initially, hydrostatic forces deposited the distributed rod-like CNC on the filter membrane randomly and fast (30 s), generating a film-like gel that reduced the flow rate of water. As a result of the slower filtering velocity, the CNC had more time to self-assemble into liquid crystals structures with helical axes orientated along the hydrostatic force direction under the greater vacuum force [82]. As filtration proceeded, the number of tactoids increased until they coalesced into a long-range periodic chiral nematic structure [83]. Concurrently, the entrapment influence on the initial layer of constructed gel, combined with hydrostatic and electrostatic forces, compacted the final structure parallel to the interface. The procedure was then repeated until all of the surplus solvents were eliminated [84]. The vacuum-assisted CNC self-assembly method is depicted schematically in Figure 9.

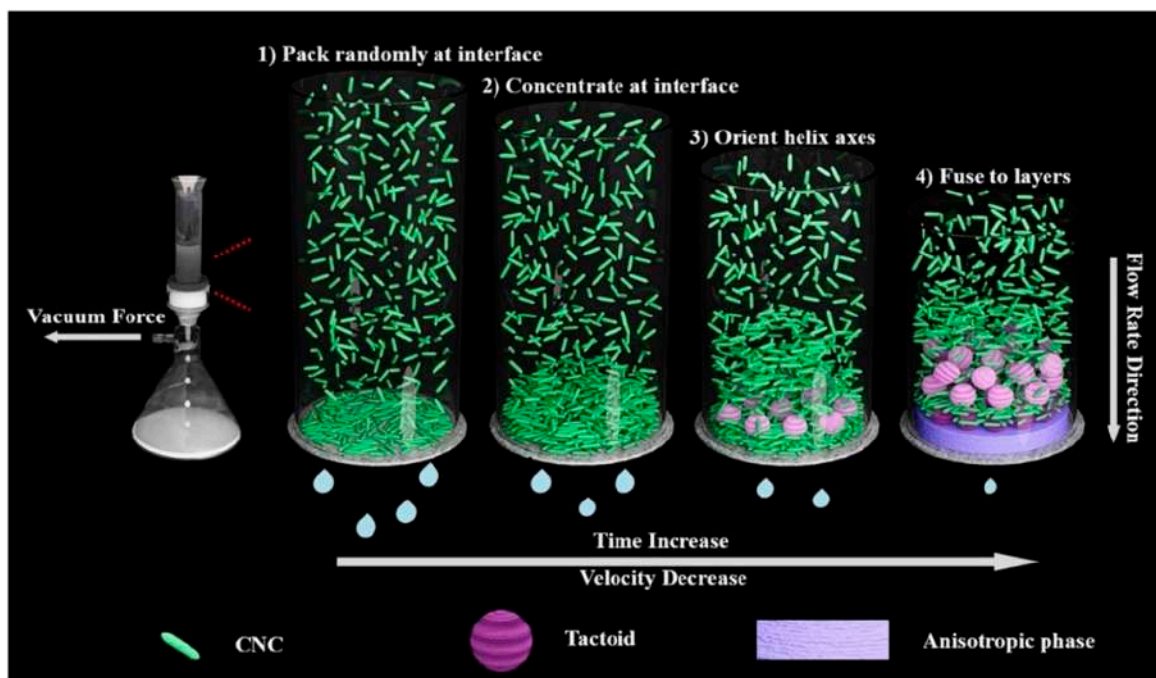


Figure 9. Schematic representation of the vacuum-assisted CNC self-assembly process. Reproduced from [82].

In addition, a suspension of 8.5% of cellulose nanocrystal can be used to prepare films with chiral nematic liquid crystals' optical properties. These films circularly reflected polarized light with a narrow wavelength that varies with the angle of viewing. The color of these films' reflections can be adjusted by adding salt to the suspension. The

CNC self-assembly into chiral nematic liquid crystalline structures did not only occur in aqueous but also in the dry state. They constructed a chiral nematic phase at high concentrations, a characteristic of liquid crystalline polymers, giving rise to attractive optical properties [85]. In the dry state, the crystalline phase of chiral nematic liquid can be preserved. In addition, the color formation dynamics can also be varied by altering the film formation environment [86].

4.1.2. Evaporation Induced Self-Assembly (EISA)

Evaporation-induced self-assembly is a method of synthesis where a drop of solvent is applied to the elements to be assembled and left to dry naturally in the air. Individual components spontaneously associate into an organized pattern or structure as a result of solvent evaporation. The maximum reflection wavelength is related to the pitch P using Braggs' formula, $\lambda = n_{av}P\sin\theta$, where n_{av} denotes the average refractive index of the crystalline material (1.56 for CNC), and θ represents the incidence angle of circularly polarized light on the film surface [87]. The quality of the film depends on CNC orbital shear, concentration, drying conditions, and surface anchoring. CNC films of large planar domains were fabricated by slowly drying CNC dispersions placed between two glass surfaces in a water vapor-saturated environment on an orbital mixer. These domains exhibited the double peaks reflectance spectra biomimetic feature like in *Lomaptera* beetles [88].

The liquid crystalline phase emergence was observed by Jativa et al. in the constrained space of an isolated and shrinking CNC-containing droplet soaked in a binary toluene-ethanol mixture (Figure 10). The shrinking droplet's contact angle with the hydrophobized substrate was so high (155°) that it resulted in the preservation of the droplet's spherical shape throughout the drying process [89].

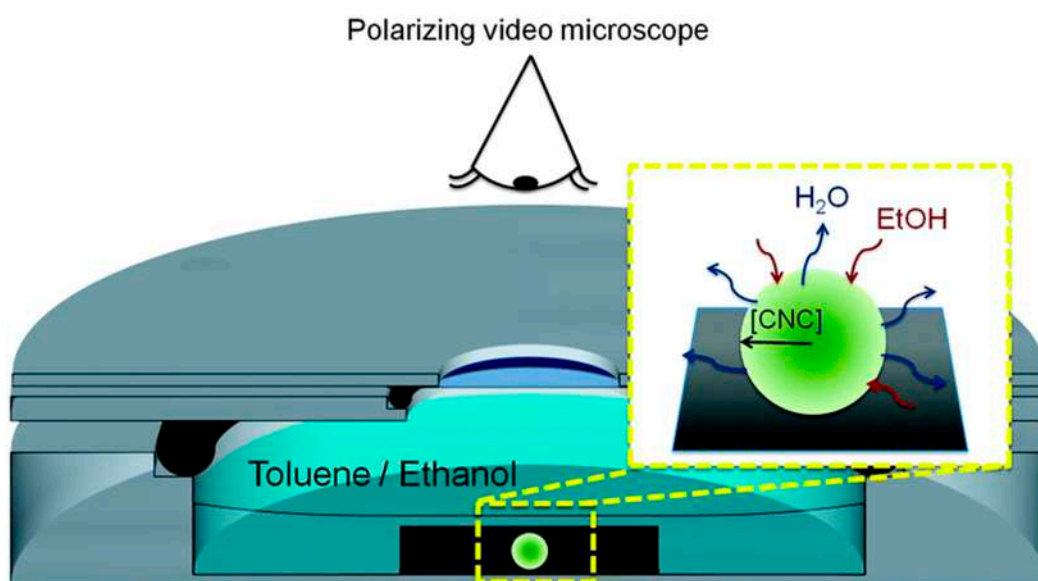


Figure 10. The cell utilized for polarized video microscopy imaging of the decreasing droplets is shown schematically. The CNC droplet (bright green) is captured in reflection mode on a hydrophobic OTS-silicon substrate (black). Water and ethanol diffusion and the resulting radial CNC concentration gradient are depicted. Reproduced from [89].

4.1.3. Functionalization of CNC for Self-Assembly

Nanocellulose in its natural form has limitations in several applications, including as a biomimetic. Modification via surface functionalization is a critical step in enhancing biocompatibility functions in a variety of applications. This can be accomplished through a variety of surface functionalization strategies, the majority of which incorporate the chemistry of hydroxyl function. Additionally, as illustrated in Figure 11, a search on lens.org using the keyword “functionalization of nanocellulose” revealed an increase in

the number of manuscripts putting the focus on nanocellulose functionalization in recent years. As a result, this demonstrates that investigation on nanocellulose functionalization has maintained a high level of interest among scientists over the last decade.

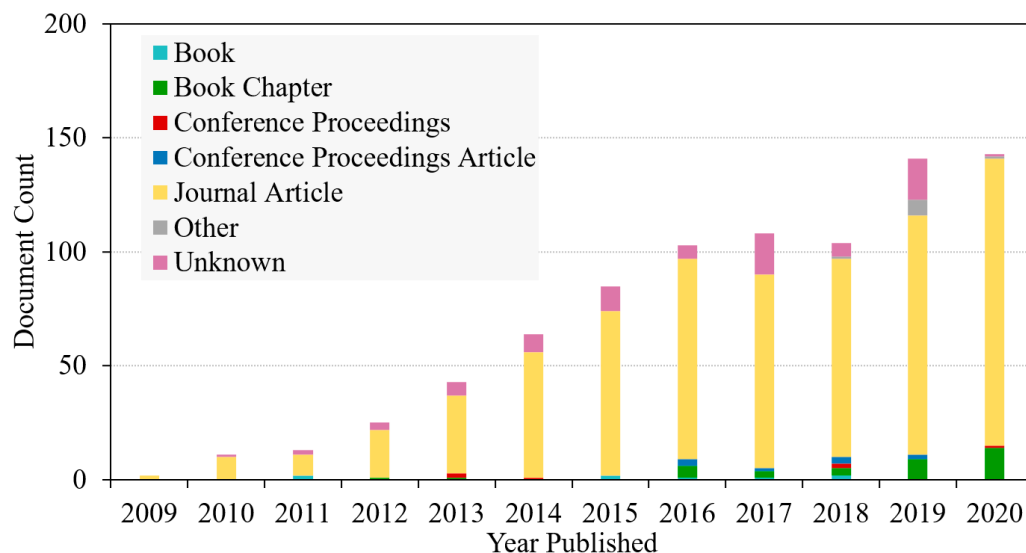


Figure 11. A chart of published manuscripts on the nanocellulose functionalization from [Lens.org](#), accessed on 15 February 2021.

For the CNC functionalization, usually, 12% acrylamide was grafted on CNC, which self-assembled into chiral nematic suspension at 3% content [90]. The liquid crystals properties analysis was performed using polarizing optical microscopy. The acrylamide grafted nanocellulose was self-assembled to a lyotropic state. The formation of liquid crystals' structure was because of the attractive Van der Waals forces and repulsive electrostatic forces [90]. An electrolyte like NaCl was added to CNC suspension before evaporation took place to produce colored films. CNC films can also be produced using spin coating on mica wafers. The electrolyte addition like NaCl to chiral nematic CNC suspensions reduces the pitch values to prepare iridescent films of the desired wavelength.

The CNC films' colors can be changed by adjusting the chiral nematic pitch P of cellulose nanocrystal. The addition of glucose increased the pitch and shifted the color to the spectrum's red end in the final film [91]. Grafting the CNC with a charged organosilane and functionalizing using a counter-ion polyoxyethylene ether resulted in the formation of liquid crystals nature. This suspension possessed a bright birefringence between the crossed polarizers at room temperature [92]. Figure 12 shows 6% CNC suspension as viewed from polarized light microscopy [93].



Figure 12. The 6% CNC suspension as viewed from polarized light microscopy [93].

4.2. Sacrificial Templates

Sacrificial templating is the most extensively utilized technique for generating nanocellulose-based porous materials because of the variety of fabrication processes that fall under this category, as well as the range of pore sizes/morphologies that may be achieved. This method entails creating a template within a nanocellulose solution or gel that may then be varied to generate a variety of pore morphologies and then eliminated using different methods. In most cases, a solvent, e.g., water, is employed in sacrificial templating, although care must be given to avoid pore collapse when the solvent is removed. As a result, the supercritical or freeze-drying method is frequently utilized to assure pore stability in final porous materials. In reality, the used drying procedure is significantly affecting the shrinkage, porosity, density, and pore size. Specific surface area, interconnectivity, and size distribution of the material: smaller pores are frequently the result of supercritical drying (usually micro and mesopores) versus freeze-drying, resulting in macroporous analogs [94].

These chiral nematic structures are embedded into silica, organo-silica, hydrogels, thermoset phenol-formaldehyde, and amino formaldehyde resins. Selective removal of nanocellulose can be used as a sacrificial template to produce materials like mesoporous silica. These types of mesoporous materials are useful in stereospecific catalysis, chiral separation, photonic materials, and chiral recognition (sensing). By minor changes in the synthetic environments, the peak reflected wavelength of the free-standing films could be differed across the whole visible and into the near-infrared spectra [95].

Introducing porosity into photonic crystals can tune their optical properties. The lyotropic liquid crystals self-assembly has been employed to introduce mesoporosity into photonic crystals, where these materials are used in the refractive index-based photonic sensors. CNC can be used as a template to create mesoporous structures. The CNC removal from CNC/silica composite was performed by calcination or by acid hydrolysis [96]. A composite of CNC and a urea-formaldehyde resin was formed, which underwent rapid and reversible color changes upon swelling can be used for pressure sensing application. At 700 °C, alkaline treatment of the composite films with 15% aqueous KOH removed the urea-formaldehyde, resulting in insoluble and luminescent cellulose films (mesoporous photonic cellulose films) [97]. The preparation of chiral nematic mesoporous carbon was performed via polymerization of polyacetylene within thermotropic chiral nematic liquid crystals, doping with iodine, and pyrolysis, displaying attractive electromagnetic characteristics [98].

5. Formation of Flexible CNC Films

To expand the applications of CNC, CNC is dispersed in organic solvents. These nanoparticles exhibit lyotropic liquid crystalline behavior in suspension, which refers to phase changes from an isotropic liquid to an ordered liquid crystal as the concentration changes. Indeed, a chiral nematic phase form exists above a certain concentration; meanwhile, within certain conditions, the suspension can be slowly evaporated, forming semi-translucent films that retain the order of the chiral nematic liquid crystals formed in the suspension. These films demonstrated iridescence when reflecting polarized light in a narrow wavelength range as determined by the films' refractive index and chiral nematic pitch. These aforementioned CNC's optical behaviors are potentially generating wider CNC films applications. Ultrasound treatment was found to increase the chiral nematic pitch in suspension and red-shift the reflection wavelength of CNC films as the applied energy increased.

In the film formation, CNC is first treated with a base and freeze-dried. This broadens the application possibilities for novel photonic materials prepared via CNC templating. Tape casting, also known as knife coating and doctor blading, is a process where a thin layer of ceramic slurry is cast onto a flat surface, dried, and sintered, which can also be used for preparing CNC films. This method is very effective in aligning CNC. Variables like pH, drying conditions, type of substrate, and CNC concentration are tuned to achieve different orientations in CNC films. Thus, CNC films exhibit both ceramics-like as well

as polymer-like properties, which are based on film orientation. The color of CNC films is affected by changing the helical pitch, and tweaking this structural color has been an ongoing topic of interest for several research groups in the previous decade.

The films formed with CNC are usually brittle. To increase the films' flexibility, some synthetic polymers can be added. The addition of polyethylene glycol (PEG) increased the flexibility of CNC film with a doubling of the elongation, and the color of the film was preserved [99]. Self-organization resulted in Bragg's reflection of visible light from the dried films. Iridescence and colored films are only possible if the pitch length of the solid films is equivalent to the visible light wavelength [88].

Glycerol can be used as both a hygroscopic agent and plasticizer to produce controllably iridescent, flexible, and multi stimuli-responsive CNC film. The CNC self-assembly in an aqueous solution was not affected by the additive but made it free-standing. These films can change color structurally in response to mechanical compression and environmental humidity, where the colors were due to the interference of light in intermittently layered or lattice structures. These films find applications in anti-counterfeiting technology, colorimetric sensors, as well as decorative coatings [100]. Zwitterionic surfactants with nanocellulose can form flexible and iridescent films. Zwitterionic surfactants can connect neighboring CNC. When the ratio of the Zwitterionic surfactant was increased, there was a shift towards a higher wavelength [101].

The CNC/waterborne polyurethane (WPU) composite papers showed optical responses to wet gas and water. Thereby, chiral nematic structured CNC-derived photonic papers with rapid stimulus-response, rewritable efficiency, and high flexibility are prepared. The chiral nematic structure retention is very sensitive to ionic strength and pH value [102]. The CNC and glycerol are added in different compositions of 100/0, 90/10, 80/20, 70/30, 60/40, and 50/50 to produce intelligent, responsive iridescent films. The glycerol addition enhanced the mechanical performance and crystallinity of the composite films [103]. The CNC/PEG (80/20) composite film was used as a humidity sensor, which showed green to transparent color change for relative humidity (RH) between 50 and 100% due to the reversible chiral nematic structure's dehydration and swelling [103].

In contrast, self-assembly of the chiral nematic consists of pseudo layers, where the CNC was aligned along with a director, and each director's orientation was slightly rotated about the helicoidal axis from one layer to the next. The pitch (P) is the vertical distance necessary to finish a 180° rotation of the director. These films reflected only left-hand circularly polarized light and exhibited distinct differently colored domains. Scanning electron microscopic (SEM) images confirmed that the pitch is well-defined within the domains of a single color [85]. The nanocellulose films' optical properties were analyzed in the wavelength range of 200–1000 nm for the regular light transmittance with a UV-visible spectrometer. The densely packed cellulose nanofibers resulted in films that were optically transparent; hence, the interstices between the fibers were sufficiently small to prevent light scattering. The 600 nm transmittances of soft and hardwoods TEMPO-oxidized films were observed at approximately 90% and 78%, respectively [52].

6. CNC-Based Liquid Crystals in Biomimetic Applications

Nature-based nanomaterials like nacre, bone, wood, butterfly wings, and beetle scales inspire man to apply the biomimetic approach to develop new multifunctional materials [23]. Nature's brightest and most colorful materials, such as peacock feathers, butterfly wings, and opals, derive their color exclusively from their internal structure. Self-assembly of CNC to a chiral nematic (cholesteric) liquid crystals phase with a helical arrangement forms films with a photonic bandgap. When immersed in water, the rod-like CNC self-assembled into nanostructured layers that reflected the light of a particular color selectively. The reflected color is influenced by the layers' dimensions. Varying the humidity during film formation changes the color [99]. Bio-inspired photonics is the genesis of the development of novel and multifunctional photonic materials. CNC has been in the limelight to produce nanostructure crystals-based photonic materials that yield iridescence [104].

Additionally, manipulating the spiral orientation of CNC may result in an improvement in mechanical qualities [105].

6.1. Photonic Applications of CNC

There are several photonic structures in nature that produce bright colors and serve as inspiration for the development of a broad range of artificial photonic materials. Unlike colorant-based pigmentation, structural colors result from light interference in periodic layered or lattice structures seen in insects, fish, birds, fruits, and leaves. Photonic crystals, Bragg stacks, and chiral nematic liquid crystals have all been explored in the last several decades to generate artificial structural colors based on these fascinating phenomena [106]. Because of their iridescence properties, CNC-based optical materials have the potential to replace hazardous dyes in cosmetics, food, art, textiles, security indicators, and sensors, among other applications, in the near future.

Natural photonic nanostructures, e.g., CNC liquid crystals, have the potential to generate vibrant colors. Since the insertion of sulfate ester groups to the surface of this compound, it has been well dispersed in water, and the electrostatic repulsion that results from this allows the creation of chiral nematic liquid crystals to occur [107]. To fabricate solid films with changeable iridescent colors, this liquid crystal may be employed that uses the helical pitch to position it in the visible wavelength area when an electric field is applied (Figure 13) [108]. This model suggests that the helical pitch orientation is critical in determining the incoming light's maximum reflected wavelength [109]. The CNC can easily arrange into photonic structures with the correct helical orientation, resulting in the development of advanced optical materials.

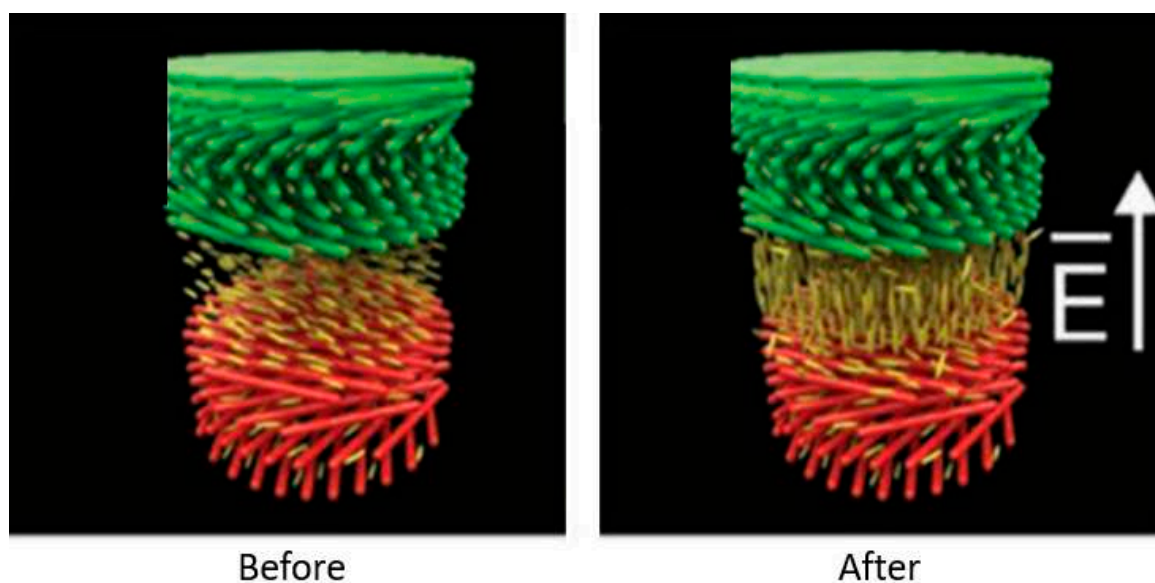


Figure 13. The orientational effect on CNC after an electric field (E) is applied to a 5CB positive dielectric nematic layer. Adapted from [108].

To produce highly ordered superlattices and helicoidal structure networks whose pitch is in the visible wavelength range, self-assembly of colloidal nanocrystals following solvent evaporation is critical (Figure 14a) for CNC iridescent film fabrication [110]. Previously published work has shown that the iridescence of CNC films may be tuned by altering the pitch of the CNC dispersion through sonication to control the helical orientation of the chiral nematic phase [111]. Before film casting, ultrasonic energy increases the chiral nematic phase suspension pitch and shifts the resulting iridescent film's reflection band to long wavelengths (Figure 14b). In the sample, the energy input per gram of CNC (degree of sonication) affected the amplitude of reflection band red-shift (reflection wavelength), and these effects of sonication on treated CNC suspensions were certainly permanent and

cumulative. Figure 14c shows the evolution of the film's conductivity and peak reflection wavelength as a function of the applied ultrasonic energy for a CNC suspension. An electrolyte added to the solution reversed the sonication's effects, causing a blue shift in the reflection wavelength that could be used to control the film's reflectivity. Surface charge density and other CNC parameters like particle length do not seem to have an impact on this effect [111].

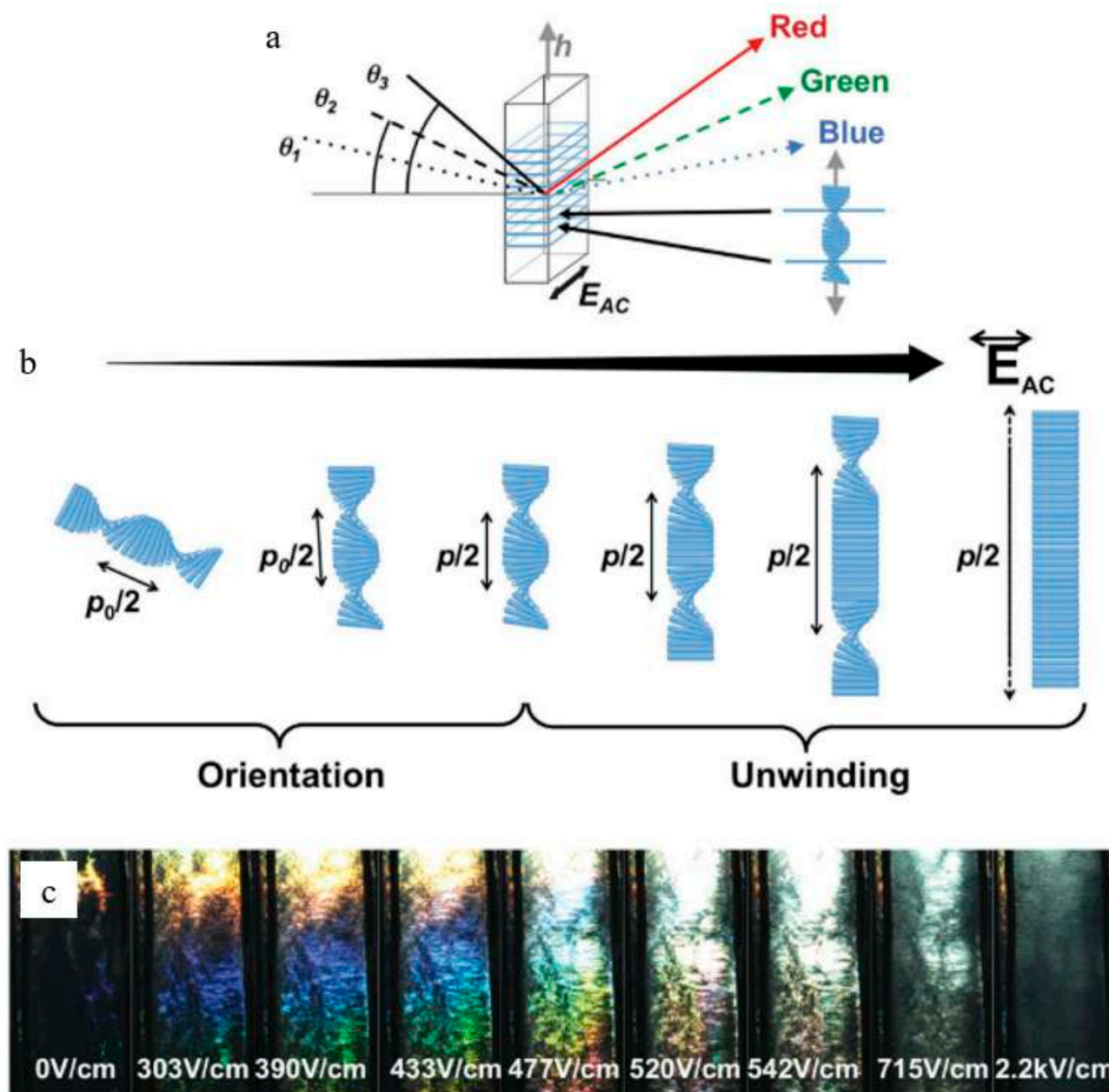


Figure 14. (a) Iridescence schemata, (b) cholesteric orientation and unwinding sequences upon the increase in the electric field, and (c) iridescence evolution upon electric field application (values in rms), demonstrating increased in light intensity, then redshift, and lastly color disappearance. Reproduced from [110].

In Chen and colleagues' research [109], the iridescent chroma of CNC films may be controlled by sonication duration, suspension volume, and degree of vacuum. Chen and colleagues discovered that films made from CNC suspensions with longer average particle lengths reflect more redly, whereas films made from shorter CNC particles reflect more blue. Given that sonication has the capability of shortening the CNC particles, it increases

the pitch of the chiral nematic phase, causing a red shift in the reflection wavelength of the resultant solid iridescent film. When the sonication time exceeds 10 h, a distinct iridescent color is shown in Figure 15a. Longer sonication increases the brightness of the resultant film, as well as its color. While samples treated for short periods of sonication (7 and 10 h) did not exhibit any noticeable reflection peak in the wavelength range of 300–800 nm of UV-Vis spectra, longer periods of sonication (i.e., 12 and 15 h) revealed reflection peaks, which were blue-shifting with increasing sonication time. A linear connection between the film thickness and the volume of the CNC suspension is seen in Figure 15b. This suggests that the volume of the CNC suspension may be carefully regulated to get precisely controlled thicknesses of iridescent films (as the film's thickness may attribute to iridescence). With increasing vacuum pressure (from 0.07 to 0.04 MPa), the iridescent color varies, as seen in Figure 15c. This finding implies that the iridescent color is likewise vacuum dependent.

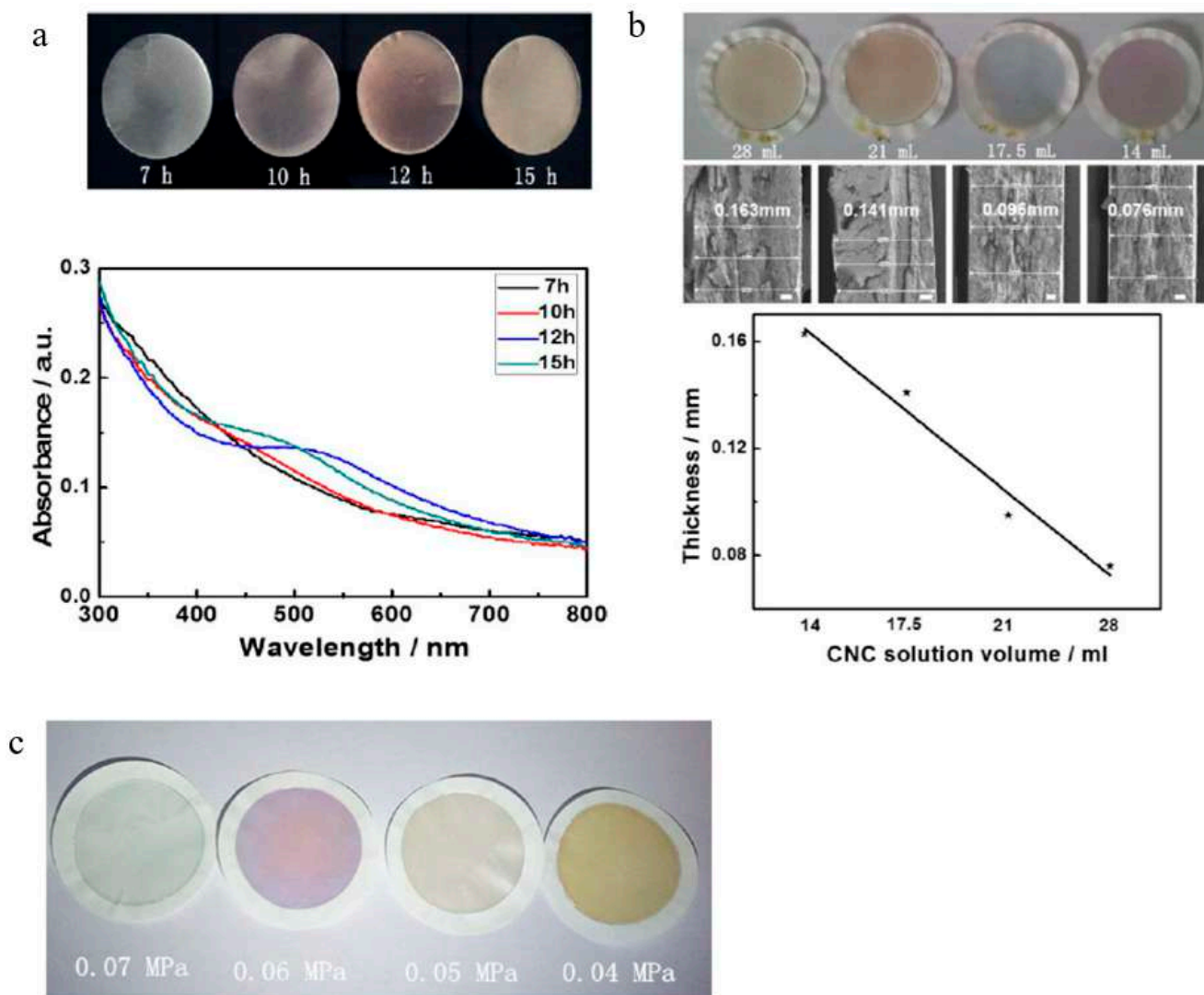


Figure 15. (a) Photographs of CNC iridescent solid films prepared with varying sonication times and their UV-Vis spectra; (b) optical photographs of CNC iridescent solid films prepared with varying CNC suspension volumes and their SEM images of the cross-sections, and a plot of film thickness as a function of CNC suspension volume; (c) photographs of CNC iridescent films prepared with various degrees of vacuum. Reproduced from [109].

Using a glycerol-derived plasticizer and a hygroscopic ingredient for CNC, He et al. [106] developed flexible and multi-responsive chiral nematic films that were inspired by the color shift of longhorn beetles *Tmesisternus isabellae* from golden in the dry state to red in

the wet state. The quantity of glycerol used changed the iridescent color of these films from blue to red. These CNC/glycerol films were photographed vertically, as shown in Figure 16a, where distinct iridescent colors can be observed as the concentration of glycerol increases. This has been linked to the fact that light of a certain wavelength is lost when it passes by these films. By using UV-Vis, it was found that the addition of glycerol results in a progressive red shift of the maximum extinction wavelength from 347 nm to 610 nm (Figure 16b). Furthermore, the inclusion of glycerol gives the CNC films a high degree of flexibility, allowing them to be bent and stretched with an elongation-at-break exceeding 2% (Figure 16c). Reversible color changes are seen in the films when they are subjected to a range of relative humidity levels (Figure 16d). In light of the aforementioned characteristics and functionalities, it is anticipated that CNC films will find applications in colorimetric sensors, anti-counterfeiting, and aesthetic coatings.

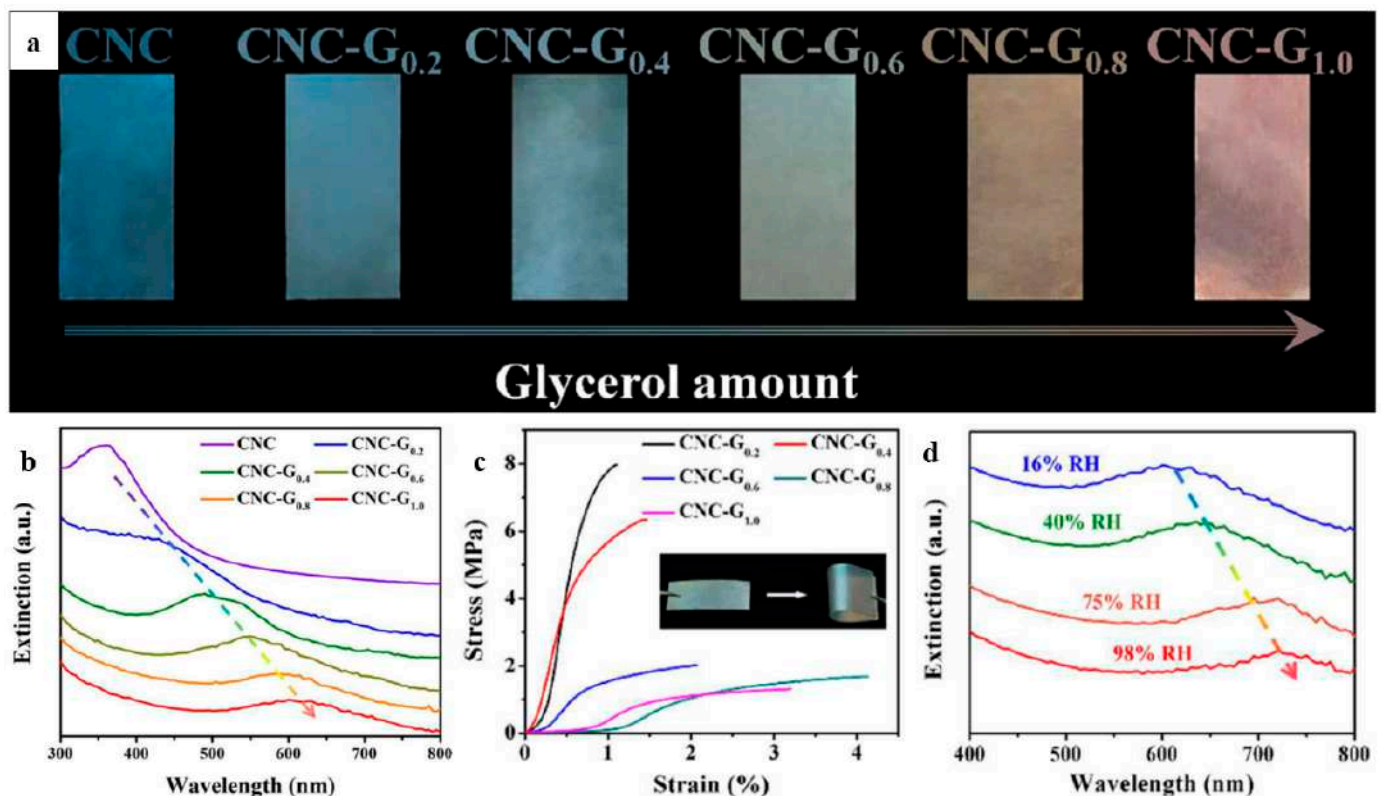


Figure 16. (a) Photographs of CNC films prepared with varying glycerol concentration; (b) UV-Vis spectra of the resultant CNC/glycerol films; (c) tensile property of CNC/glycerol films; and (d) effects of humidity-responsive CNC/glycerol films. Reproduced from [106].

CNC's macroscopic characteristics are greatly influenced by its microscopic characteristics (rheology, colloidal stability, etc.). Modifying and functionalizing CNC are likely to improve colloidal stability with the addition of a surfactant or surface functionalities, which leads to the development of new and better materials with advanced capabilities. The inclusion of hydroxypropyl cellulose (HPC) into a CNC film made by slow evaporation was investigated by Walters and colleagues [112]. Changes in HPC concentration or molecular weight modulated the color over the visible spectrum (Figure 17a), and composite films were more flexible than neat CNC film, with a tenfold increase in elasticity, but decreased in stiffness and tensile strength (Figure 17b–d).

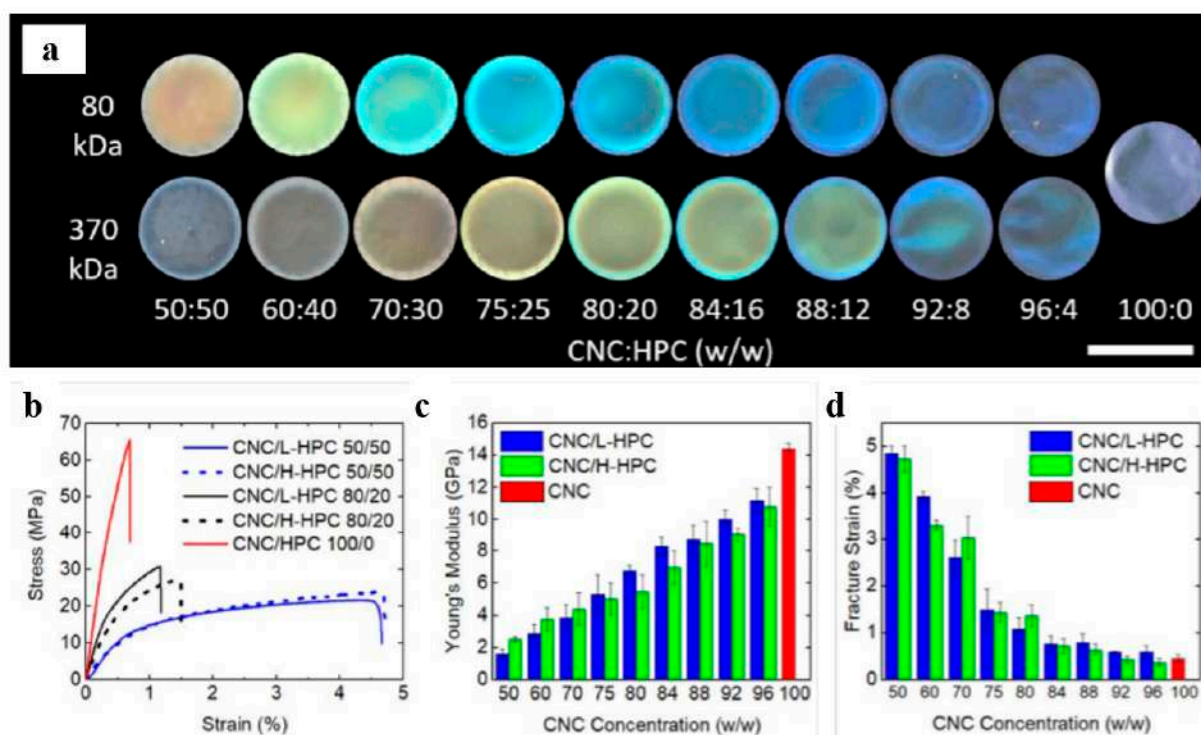


Figure 17. (a) Photographs of iridescent films prepared with varying molecular weight and HPC concentration (scale bar, 3.5 cm); (b) stress–strain curves for different CNC/HPC composite films; (c) Young’s modulus for different CNC concentrations for both H-HPC (370 kDa) and L-HPC (80 kDa) composite films; (d) fracture strains for different CNC concentrations for both H-HPC and L-HPC composite films. Reproduced from [112].

An optically transparent clear paper with >90% transmittance and haze value <1% has also been discovered [113]. Transparent cellulose paper is a photonic material for flexible electronics, optoelectronics, and photonics with the potential to replace SiO₂. Mesoporous materials are the materials through which photons can be manipulated. Mesopores can be filled with high refractive index materials to create photonic structures. When cellulose nanofibers are densely packed, this transmittance >90% and haze value <1% can be achieved. Nano welding of fibers in ionic liquids gives much denser packing. With graphene oxide/cellulose crystal composites, proximity sensors with a faster response time and increased sensitivity can be developed. The composite’s high optical transparency and sensing capability enable it to be used in touch and non-touch screens in portable entertainment units, mobile phones, human skin, robotics, and explosive environments while consuming little energy.

Thermo-responsive photonic films with CNC and poly diol citrate elastomer have also been discovered by Espinha et al. (2016). Although cellulose-derived photonic structures possessed intense color, they demonstrated brittle structure. Poly diol citrate provided flexibility and enhanced functionality by giving the shape memory effect. Other polymers like polycaprolactone and PEG can also be used for this purpose. The materials integrated mesoporous photonic cellulose’s chiral nematic structural properties with the magnetic characteristic of cobalt ferrite. The dielectric feature significantly improved as a result of the mesoporous films’ effective swelling ability, an interesting feature for the application of electromagnetic interference shielding.

CNC-based aerogels are tough and flexible mechanically, optically transparent, and highly porous. They are suitable for applications requiring a fire-resistant, direction-dependent mechanical or electrical insulator. Birefringent inks made from CNC are applied in optical authentication and security printing. When printed on dark paper, these inks produce letters that are darker than the background without polarizers and brighter than

the background with crossed polarizers [114]. Multifunctional biomimetic materials and sensors can be constructed using CNC/graphene composites. The color of the film can be altered by hydration or dehydration, similar to how beetles *Tmesisternus isabellae*'s elytra respond to water. The cracking and coffee ring effect of the CNC film can be avoided by the process of vacuum-assisted self-assembly. CNC coatings are made with aqueous CNC solutions that have applications in several colorants, UV-curable water-based clear coating formulation, and specific additives in clear coatings for wood. CNC liquid crystals membrane can be obtained by evaporating the cellulose nanocrystal at 20–80 °C for 1–12 h. This membrane is applied in wide practices, such as decoration, anti-fake labels, color coatings, and temperature sensors or optical verification equipment.

6.2. Hydro-Responsive Materials

In plants, bending and unbending motions caused by humidity constitute motivation for the development of new biomimetic materials. Even in the tissues of dead plants, similar motions have been documented. The development of anisotropic cellulose-based micro/nanostructures are engineered to alter form as environmental conditions change, forming the basis of the responsiveness of these materials [115]. Humidity-responsive, bioinspired, CNC-based sandwich assembled composite photonic film with a left-handed chiral nematic structure was reported by Wu et al. (2016). The asymmetric composite film was fabricated by stacking hydrophilic CNC and poly(ethylene glycol) diacrylate (PEGDA) layers, with the polyamide-6 layers being oriented in a uniaxial direction. Asymmetric swelling of the hydrophilic sandwich components, namely CNC and PEGDA, caused the cellulose composite film to contract once subjected to humidity. These results might be explained by the fact that an increase in helical pitch near the moisture source causes an asymmetrical expansion of sandwiched structure nanocomposite film (Figure 18), hence allowing swelling on the stimulated side but no changes on the opposite side.

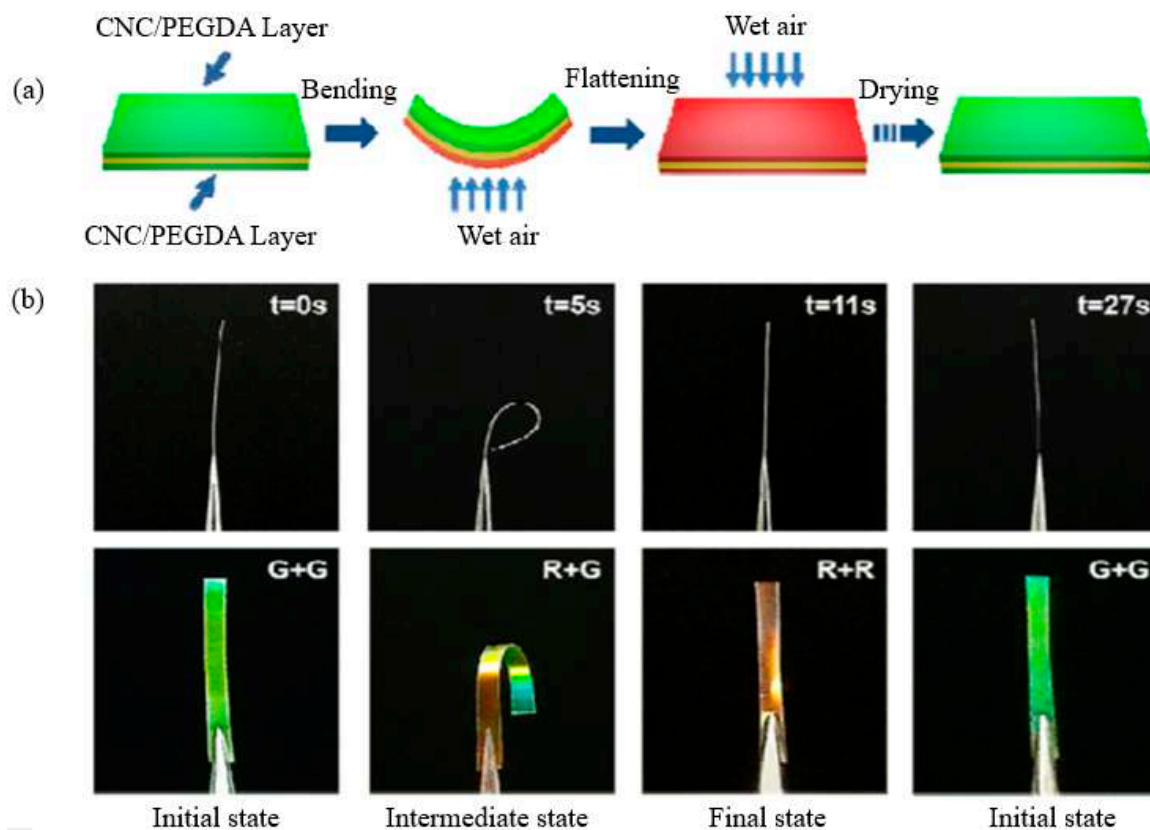


Figure 18. (a) Water vapor-based actuation in a sandwiched structure nanocomposite film is shown schematically; (b) images of the sandwiched nanocomposite film deformation and coloration. Reproduced from [116].

6.3. 4D Printing Materials

4D printing is a one-step process in which several properties of materials can be combined to allow the conversion of a 1D strand or 2D surface into a 3D shape, or even the transformation of a 3D shape into another 3D shape, using, for example, only water as the activator. 4D printing is becoming increasingly popular as a method of prototyping new materials. Using this printing process, manufacturers are able to produce and manufacture intelligent, reconfigurable materials that are better suited to specific uses [117].

3D printing of renewable building blocks, for example, CNC, provides an appealing method of producing environmentally friendly materials. Anisotropic CNC-based viscoelastic inks were developed by Siqueira and colleagues to provide direct ink writing patterning of 3D objects [118]. The printing efficiency has been shown with a monomer-based ink that is constituted of CNC dispersed in a solution including 2-hydroxyethyl methacrylate (HEMA) monomer, polyether urethane acrylate, and a photo-initiator, which is cured by ultraviolet light. Anisotropic components were aligned and stiffened along the printing direction in structures printed using CNC-based inks, demonstrating shear-induced alignment of the anisotropic elements (Figure 19). As a result of these characteristics, CNC-based inks are promising candidates for biomimetic 4D printing of programmable reinforced materials that adapt to environmental stimuli.

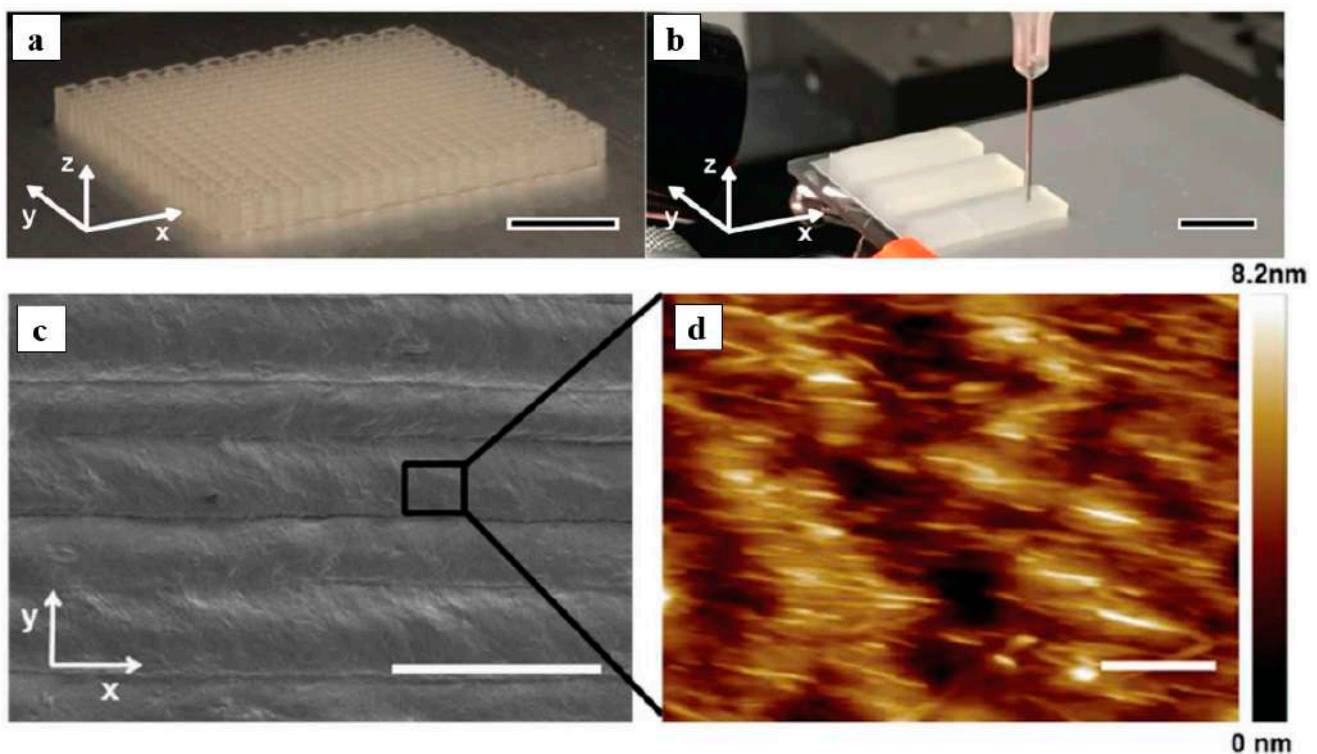


Figure 19. (a,b) Photograph of 3D printed grids and blocks with eight layers of parallel lines; (c,d) CNC alignment in 3D printed films: SEM (scale bar, 200 μm) and AFM topologies (scale bar, 100 μm). Reproduced from [118].

6.4. Bone Substitute Materials

It has been decades since researchers started experimenting with synthetic materials that match real bone composite in chemical and structural features [119]. Therefore, new varieties of 3D scaffolds have been developed in response to the intrinsic relationship between hydroxyapatite (HAP) and human bone to address the shortcomings of presently used bone replacements [120].

Huang et al. [121] created a novel nanocomposite scaffold by homogeneously depositing hydroxyapatite atop a cellulose nanocrystals matrix floating in simulated body

fluid (SBF). The HAP content of the nanocomposite may be adjusted from 15% to 47% by varying the pH of the SBF. Through the use of the directional freezing (DF) method and lyophilization, the nanocomposites were freeze-casted into porous scaffolds. According to the results of compression tests on the HAP/CNC foams, compared to standard freezing procedures, this solidification approach significantly improved mechanical qualities because of the unique orientation and anisotropic porous structure. Ice crystals grew vertically in response to the DF temperature gradient, forcing them to grow vertically. The procedure created a channel structure that was directed and continuous in respect to the compression force (Figure 20). The scaffold with a high HAP concentration had demonstrated better mechanical and thermal capabilities, suggesting that it may have the potential for use in bone tissue engineering.

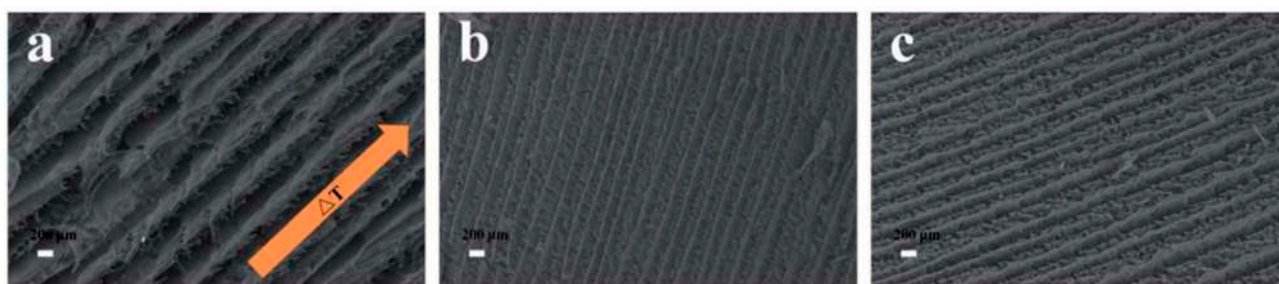


Figure 20. (a–c) Using the directionally frozen approach, SEM images of the longitudinal side views of freeze-casted porous foams were identified on the long axis. Reproduced from [121].

6.5. Nanocomposites

The relationship between mechanical properties of natural fibers and nanoscale structural orientation of CNC is of particular interest from the perspective of polymer nanocomposite processing because they provide an opportunity to control fiber mechanical properties by tailoring the self-assembly of nanoparticles within the polymer matrix. Research has shown that this structure–property relationship appears in CNC reinforced fibers. The mechanical characteristics of the fiber may be adjusted by regulating the CNC weight fraction loading and the fiber wet-spinning qualities. The mechanical properties of the fiber are closely related to the CNC spiral angle inside the fiber.

Using a biomimetic approach, Esteban and colleagues [105] developed polymer nanocomposites with controllable structure–property relationships. Adding CNC to alginate fiber increases the modulus at high loading CNC, as shown by the nanocomposite tensile characteristics for constant J_A . These results imply that this phenomenon might be a result of the creation of a CNC percolation network across the fiber. Even at modest loads, adding CNC improved fiber toughness and elongation at break hence allowing for wet spinning of nanocomposite fibers to be carried out at a higher J_A , doubling the fiber output rate. When the CNC concentration is high enough, the spiral angle seems to develop; however, higher levels of J_A hinder the spiral structure’s emergence but encourage alignment along the fiber axis instead.

Another study by Fernandes et al. [122] introduced a low loading of CNC into liquid-crystalline HPC, resulting in a significant increase in mechanical features without compromising the composite liquid-crystalline order. There were two similar sets of bands detected in low concentration CNC/HPC films, which were studied by AFM (Figure 21a–c). It concluded that while CNC facilitates the reinforcement of the composite, the development and periodicity of the bands are primarily dictated by the chiral nematic-liquid-crystal characteristics imposed by the initial precursor solution as well as the processing parameters.

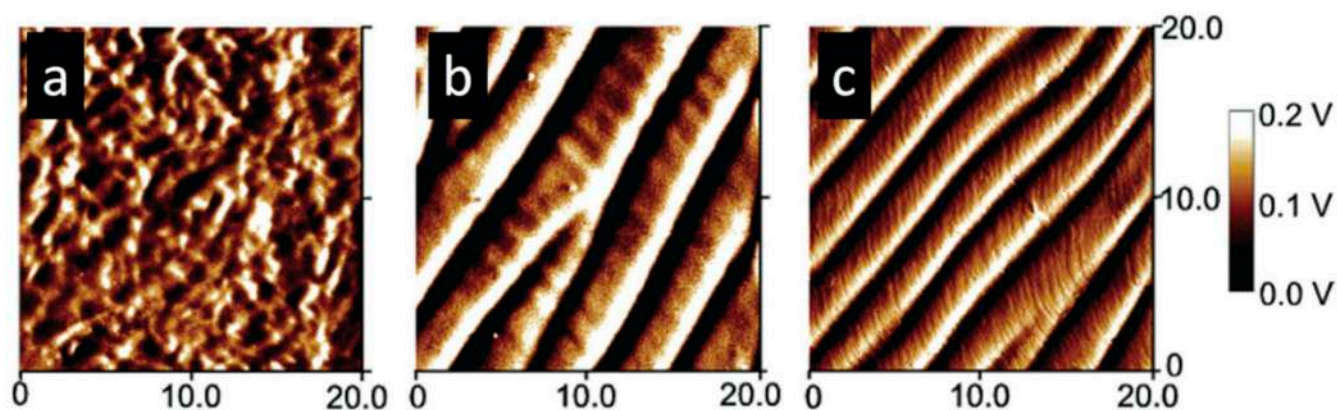


Figure 21. AFM top-view images CNC/HPC sheared films (shear rate 5 mm s^{-1}) from (a) isotropic and (b,c) liquid-crystalline solutions. Reproduced from [122].

7. Conclusions and Future Recommendations

Nanocellulose can be extracted from cellulosic materials via the acid hydrolysis process in which the disordered regions are hydrolyzed by acid and the ordered portions are left. The self-assembly of CNC in aqueous solutions brings out many colors called iridescence due to its photonic structures. Nanocellulose is able to replace glass in optoelectronic devices by tailoring its optical properties. The pitch of CNC can be varied by introducing various electrolytes in it. CNC shows high transparency in the visible region. These optical properties are useful to make humidity sensors. The CNC has been found to be a green material to develop more functional materials that are birefringent. Additionally, some difficulties associated with nanocellulose have been identified. CNC necessitates high production costs, particularly at industrial levels. The chemical and energy consumption associated with the manufacture of CNC continues to be a bottleneck in the scale-up of nanocellulose production. However, to the best of our knowledge, progress has been made in this area, with many pilot-scale production facilities and a more environmentally friendly approach to CNC production now available worldwide. Nevertheless, the use of CNC in biomimetic applications is still limited. Therefore, more studies are needed to enhance the potential of CNC for other various fields.

Author Contributions: Writing—original draft preparation, T.T., R.A.I., T.S.M.K., S.S., M.N.F.N., M.S.M.M. and M.R.M.A.; writing—review and editing, T.T., R.A.I., T.S.M.K., S.S., M.A.A.F., M.N.F.N., M.S.M.M., N.M.N., S.Z.S.Z. and M.R.R.; funding, S.Z.S.Z. All authors have read and agreed to the published version of the manuscript.

Funding: This research was funded by Universiti Kebangsaan Malaysia (UKM) for the financial support through research grants, PP/LESTARI/2022, XX-2020-010 and GP-2021-K012939. The authors would also like to express gratitude for the financial support received from Universiti Teknologi Malaysia, project “CRG 30.3: Retardant coating using graphene/bamboo aerogel mixtures on SAR robotics system, grant number PY/2020/03495—R. J130000.7351.4B534”. The research has been carried out under the program Research Excellence Consortium (JPT (BPKI) 1000/016/018/25 (57)) provided by the Ministry of Higher Education Malaysia (MOHE).

Institutional Review Board Statement: Not applicable.

Informed Consent Statement: Not applicable.

Data Availability Statement: The data presented in this study are available on request from the corresponding author.

Acknowledgments: The author also would like to thank Universiti Kebangsaan Malaysia (UKM), Universiti Pertahanan Nasional Malaysia (UPNM), and Universiti Teknologi Malaysia (UTM) for financial, work, and facilities support.

Conflicts of Interest: The authors declare no conflict of interest.

References

1. Wei, X.; Lin, T.; Duan, M.; Du, H.; Yin, X. Cellulose nanocrystal-based liquid crystal structures and the unique optical characteristics of cellulose nanocrystal films. *Bioresources* **2020**, *16*, 2116–2137. [[CrossRef](#)]
2. Wu, Q.-Y.; Liang, Q. Interplay between Curvature and Lateral Organization of Lipids and Peptides/Proteins in Model Membranes. *Langmuir* **2014**, *30*, 1116–1122. [[CrossRef](#)] [[PubMed](#)]
3. Lepora, N.F.; Verschure, P.F.; Prescott, T.J. The state of the art in biomimetics. *Bioinspiration Biomim.* **2013**, *8*, 013001. [[CrossRef](#)] [[PubMed](#)]
4. Fayemi, P.E.; Wanieck, K.; Zollfrank, C.; Maranzana, N.; Aoussat, A. Biomimetics: Process, tools and practice. *Bioinspiration Biomim.* **2017**, *12*, 011002. [[CrossRef](#)]
5. Wanieck, K.; Fayemi, P.-E.; Maranzana, N.; Zollfrank, C.; Jacobs, S. Biomimetics and its tools. *Bioinspired Biomim. Nanobiomater.* **2017**, *6*, 53–66. [[CrossRef](#)]
6. Hwang, J.; Jeong, Y.; Park, J.M.; Lee, K.H.; Hong, J.W.; Choi, J. Biomimetics: Forecasting the future of science, engineering, and medicine. *Int. J. Nanomed.* **2015**, *10*, 5701–5713. [[CrossRef](#)]
7. Paris, O.; Burgert, I.; Fratzl, P. Biomimetics and Biotemplating of Natural Materials. *MRS Bull.* **2010**, *35*, 219–225. [[CrossRef](#)]
8. De Souza, J.F.; Pontes, K.D.S.; Alves, T.F.R.; Amaral, V.A.; Rebelo, M.D.A.; Hausen, M.A.; Chaud, M.V. Spotlight on Biomimetic Systems Based on Lyotropic Liquid Crystal. *Molecules* **2017**, *22*, 419. [[CrossRef](#)]
9. Webber, M.J.; Appel, E.A.; Meijer, E.; Langer, R. Supramolecular biomaterials. *Nat. Mater.* **2016**, *15*, 13–26. [[CrossRef](#)]
10. Norrrahim, M.N.F.; Ariffin, H.; Yasim-Anuar, T.A.T.; Ghaemi, F.; Hassan, M.A.; Ibrahim, N.A.; Ngee, J.L.H.; Yunus, W.M.Z.W. Superheated steam pretreatment of cellulose affects its electrospinnability for microfibrillated cellulose production. *Cellulose* **2018**, *25*, 3853–3859. [[CrossRef](#)]
11. Yasim-Anuar, T.A.T.; Ariffin, H.; Norrrahim, M.N.F.; Hassan, M.A.; Andou, Y.; Tsukegi, T.; Nishida, H. Well-Dispersed Cellulose Nanofiber in Low Density Polyethylene Nanocomposite by Liquid-Assisted Extrusion. *Polymers* **2020**, *12*, 927. [[CrossRef](#)] [[PubMed](#)]
12. Asyraf, M.R.M.; Syamsir, A.; Zahari, N.M.; Supian, A.B.M.; Ishak, M.R.; Sapuan, S.M.; Sharma, S.; Rashedi, A.; Razman, M.R.; Zakaria, S.Z.S.; et al. Product Development of Natural Fibre-Composites for Various Applications: Design for Sustainability. *Polymers* **2022**, *14*, 920. [[CrossRef](#)] [[PubMed](#)]
13. Norrrahim, M.N.F.; Shah, N.A.A.; Jamal, S.H.; Yunus, W.M.Z.W.; Ernest, V.F.K.V.; Kasim, N.A.M. Nanocellulose-Based Filters as Novel Barrier Systems for Chemical Warfare Agents. *Solid State Phenom.* **2021**, *317*, 180–186. [[CrossRef](#)]
14. Alias, A.H.; Norizan, M.N.; Sabaruddin, F.A.; Asyraf, M.R.M.; Norrrahim, M.N.F.; Ilyas, A.R.; Kuzmin, A.M.; Rayung, M.; Shazleen, S.S.; Nazrin, A.; et al. Hybridization of MMT/Lignocellulosic Fiber Reinforced Polymer Nanocomposites for Structural Applications: A Review. *Coatings* **2021**, *11*, 1355. [[CrossRef](#)]
15. Norrrahim, M.N.F.; Ariffin, H.; Yasim-Anuar, T.A.T.; Hassan, M.A.; Ibrahim, N.A.; Yunus, W.M.Z.W.; Nishida, H. Performance Evaluation of Cellulose Nanofiber with Residual Hemicellulose as a Nanofiller in Polypropylene-Based Nanocomposite. *Polymers* **2021**, *13*, 1064. [[CrossRef](#)] [[PubMed](#)]
16. Norrrahim, M.N.F.; Huzaifah, M.R.M.; Farid, M.A.A.; Shazleen, S.S.; Misenan, M.S.M.; Yasim-Anuar, T.A.T.; Naveen, J.; Nurazzi, N.M.; Rani, M.S.A.; Hakimi, M.I.; et al. Greener Pretreatment Approaches for the Valorisation of Natural Fibre Bi-omass into Bioproducts. *Polymers* **2021**, *13*, 2971. [[CrossRef](#)]
17. Ilyas, R.A.; Aisyah, H.A.; Nordin, A.H.; Ngadi, N.; Zuhri, M.Y.M.; Asyraf, M.R.M.; Sapuan, S.M.; Zainudin, E.S.; Sharma, S.; Abral, H.; et al. Natural Fiber Reinforced Chitosan, Chitosan Blends and Their Nanocomposites for Various Advanced Applications. *Polymers* **2022**, *14*, 874. [[CrossRef](#)]
18. Norrrahim, M.N.F.; Ariffin, H.; Hassan, M.A.; Ibrahim, N.A.; Yunus, W.M.Z.W.; Nishida, H. Utilisation of superheated steam in oil palm biomass pretreatment process for reduced chemical use and enhanced cellulose nanofiber production. *Int. J. Nanotechnol.* **2019**, *16*, 668. [[CrossRef](#)]
19. Sharma, S.; Sudhakara, P.; Singh, J.; Ilyas, R.A.; Asyraf, M.R.M.; Razman, M.R. Critical Review of Biodegradable and Bioactive Polymer Composites for Bone Tissue Engineering and Drug Delivery Applications. *Polymers* **2021**, *13*, 2623. [[CrossRef](#)]
20. Norrrahim, M.N.F.; Nurazzi, N.M.; Jenol, M.A.; Farid, M.A.A.; Janudin, N.; Ujang, F.A.; Yasim-Anuar, T.A.T.; Najmuddin, S.U.F.S.; Ilyas, R.A. Emerging development of nanocellulose as an antimicrobial material: An overview. *Mater. Adv.* **2021**, *2*, 3538–3551. [[CrossRef](#)]
21. Yasim-Anuar, T.A.T.; Ariffin, H.; Norrrahim, M.N.F.; Hassan, M.A.; Tsukegi, T.; Nishida, H. Sustainable one-pot process for the production of cellulose nanofiber and polyethylene/cellulose nanofiber composites. *J. Clean. Prod.* **2019**, *207*, 590–599. [[CrossRef](#)]
22. Norrrahim, M.N.F.; Ariffin, H.; Yasim-Anuar, T.A.T.; Hassan, M.A.; Nishida, H.; Tsukegi, T. One-pot nanofibrillation of cellulose and nanocomposite production in a twin-screw extruder. *IOP Conf. Ser. Mater. Sci. Eng.* **2018**, *368*, 012034. [[CrossRef](#)]
23. Ilyas, R.A.; Sapuan, S.M.; Asyraf, M.R.M.; Dayana, D.A.Z.N.; Amelia, J.J.N.; Rani, M.S.A.; Norrrahim, M.N.F.; Nurazzi, N.M.; Aisyah, H.A.; Sharma, S.; et al. Polymer composites filled with metal derivatives: A review of flame retardants. *Polymers* **2021**, *13*, 1701. [[CrossRef](#)]
24. Norrrahim, M.N.F.; Kasim, N.A.M.; Knight, V.F.; Ong, K.K.; Noor, S.A.M.; Jamal, S.H.; Shah, N.A.A.; Halim, N.A.; Ilyas, R.A.; Yunus, W.M.Z.W. Cationic Nanocellulose as Promising Candidate for Filtration Material of COVID-19: A Perspective. *Appl. Sci. Eng. Prog.* **2021**, *14*, 580–587. [[CrossRef](#)]

25. Farid, M.A.A.; Hassan, M.A.; Roslan, A.M.; Ariffin, H.; Norrrahim, M.N.F.; Othman, M.R.; Yoshihito, S. Improving the decolorization of glycerol by adsorption using activated carbon derived from oil palm biomass. *Environ. Sci. Pollut. Res.* **2021**, *28*, 27976–27987. [[CrossRef](#)] [[PubMed](#)]
26. Lawal, A.A.; Hassan, M.A.; Zakaria, M.R.; Yusoff, M.Z.M.; Norrrahim, M.N.F.; Mokhtar, M.N.; Shirai, Y. Effect of oil palm biomass cellulosic content on nanopore structure and adsorption capacity of biochar. *Bioresour. Technol.* **2021**, *332*, 125070. [[CrossRef](#)]
27. Nurazzi, N.M.; Asyraf, M.R.M.; Rayung, M.; Norrrahim, M.N.F.; Shazleen, S.S.; Rani, M.S.A.; Shafi, A.R.; Aisyah, H.A.; Radzi, M.H.M.; Sabaruddin, F.A.; et al. Thermogravimetric Analysis Properties of Cellulosic Natural Fiber Polymer Composites: A Review on Influence of Chemical Treatments. *Polymers* **2021**, *13*, 2710. [[CrossRef](#)]
28. Asyraf, M.R.M.; Rafidah, M.; Ishak, M.R.; Sapuan, S.M.; Yidris, N.; Ilyas, R.A.; Razman, M.R. Integration of TRIZ, Morphological Chart and ANP method for development of FRP composite portable fire extinguisher. *Polym. Compos.* **2020**, *41*, 2917–2932. [[CrossRef](#)]
29. Lee, C.H.; Lee, S.H.; Padzil, F.N.M.; Ainun, Z.M.A.; Norrrahim, M.N.F.; Chin, K.L. Biocomposites and Nanocomposites. In *Composite Materials*; CRC Press: Boca Raton, FL, USA, 2021; pp. 29–60.
30. Ilyas, R.A.; Sapuan, S.M.; Harussani, M.M.; Hakimi, M.Y.A.Y.; Haziq, M.Z.M.; Atikah, M.S.N.; Asyraf, M.R.M.; Ishak, M.R.; Razman, M.R.; Nurazzi, N.M.; et al. Polylactic Acid (PLA) Biocomposite: Processing, Additive Manufacturing and Advanced Applications. *Polymers* **2021**, *13*, 1326. [[CrossRef](#)]
31. Nurazzi, N.M.; Asyraf, M.R.M.; Fatimah Athiyah, S.; Shazleen, S.S.; Rafiqah, S.A.; Harussani, M.M.; Kamarudin, S.H.; Razman, M.R.; Rahmah, M.; Zainudin, E.S.; et al. A Review on Mechanical Performance of Hybrid Natural Fiber Polymer Composites for Structural Applications. *Polymers* **2021**, *13*, 2170. [[CrossRef](#)]
32. Nurazzi, N.M.; Harussani, M.M.; Aisyah, H.A.; Ilyas, R.A.; Norrrahim, M.N.F.; Khalina, A.; Abdullah, N. Treatments of natural fiber as reinforcement in polymer composites—A short review. *Funct. Compos. Struct.* **2021**, *3*, 024002. [[CrossRef](#)]
33. Asyraf, M.; Ishak, M.; Norrrahim, M.; Nurazzi, N.; Shazleen, S.; Ilyas, R.; Rafidah, M.; Razman, M. Recent advances of thermal properties of sugar palm lignocellulosic fibre reinforced polymer composites. *Int. J. Biol. Macromol.* **2021**, *193*, 1587–1599. [[CrossRef](#)] [[PubMed](#)]
34. Asyraf, M.R.M.; Rafidah, M.; Azrina, A.; Razman, M.R. Dynamic mechanical behaviour of kenaf cellulosic fibre biocomposites: A comprehensive review on chemical treatments. *Cellulose* **2021**, *28*, 2675–2695. [[CrossRef](#)]
35. Petroudy, S.D. Physical and mechanical properties of natural fibers. In *Advanced High Strength Natural Fibre Composites in Construction*; Elsevier BV: Amsterdam, The Netherlands, 2017; pp. 59–83.
36. Zhou, Z.; Jaaskelainen, A.S.; Vuorinen, T. Oxidation of cellulose and carboxylic acids by hypochlorous acid: Kinetics and mechanisms. *J. Pulp Pap. Sci.* **2008**, *34*, 212.
37. Norrrahim, M.N.F.; Ilyas, R.A.; Nurazzi, N.M.; Rani, M.S.A.; Atikah, M.S.N.; Shazleen, S.S. Chemical Pretreatment of Lignocellulosic Biomass for the Production of Bioproducts: An Overview. *Appl. Sci. Eng. Prog.* **2021**, *14*, 588–605. [[CrossRef](#)]
38. Asyraf, M.; Ishak, M.; Syamsir, A.; Nurazzi, N.; Sabaruddin, F.; Shazleen, S.; Norrrahim, M.; Rafidah, M.; Ilyas, R.; Rashid, M.Z.A.; et al. Mechanical properties of oil palm fibre-reinforced polymer composites: A review. *J. Mater. Res. Technol.* **2022**, *17*, 33–65. [[CrossRef](#)]
39. Abitbol, T.; Rivkin, A.; Cao, Y.; Nevo, Y.; Abraham, E.; Ben-Shalom, T.; Lapidot, S.; Shoseyov, O. Nanocellulose, a tiny fiber with huge applications. *Curr. Opin. Biotechnol.* **2016**, *39*, 76–88. [[CrossRef](#)]
40. Klemm, D.; Cranston, E.D.; Fischer, D.; Gama, M.; Kedzior, S.A.; Kralisch, D.; Kramer, F.; Kondo, T.; Lindström, T.; Nietzsche, S.; et al. Nanocellulose as a natural source for groundbreaking applications in materials science: Today's state. *Mater. Today* **2018**, *21*, 720–748. [[CrossRef](#)]
41. Faiz Norrrahim, M.N.; Mohd Kasim, N.A.; Knight, V.F.; Mohamad Misenan, M.S.; Janudin, N.; Ahmad Shah, N.A.; Kasim, N.; Wan Yusoff, W.Y.; Mohd Noor, S.A.; Jamal, S.H.; et al. Nanocellulose: A bioadsorbent for chemical contaminant remediation. *RSC Adv.* **2021**, *11*, 7347–7368. [[CrossRef](#)]
42. Norrrahim, M.N.F.; Kasim, N.A.M.; Knight, V.F.; Halim, N.A.; Shah, N.A.A.; Noor, S.A.M.; Jamal, S.H.; Ong, K.K.; Wan Yunus, W.M.Z.; Farid, M.A.A.; et al. Performance evaluation of cellulose nanofiber reinforced polymer composites. *Funct. Compos. Struct.* **2021**, *3*, 024001. [[CrossRef](#)]
43. Ariffin, H.; Yasim-Anuar, T.A.T.; Norrrahim, M.N.F.; Hassan, M.A. Synthesis of Cellulose Nanofiber from Oil Palm Biomass by High Pressure Homogenization and Wet Disk Milling. In *Nanocellulose: Synthesis, Structure, Properties and Applications*; World Scientific: Singapore, 2021; pp. 51–64.
44. Norrrahim, M.N.F.; Yasim-Anuar, T.; Jenol, M.; Nurazzi, N.M.; Sapuan, S.; Ilyas, R. Performance evaluation of cellulose nanofiber reinforced polypropylene biocomposites for automotive applications. In *Biocomposite and Synthetic Composites for Automotive Applications*; Woodhead Publishing: Amsterdam, The Netherlands, 2021; pp. 199–215.
45. Norrrahim, M.N.F.; Kasim, N.A.M.; Knight, V.F.; Ong, K.K.; Noor, S.A.M.; Halim, N.A.; Shah, N.A.A.; Jamal, S.H.; Janudin, N.; Misenan, M.S.M.; et al. Emerging Developments Regarding Nanocellulose-Based Membrane Filtration Material against Microbes. *Polymers* **2021**, *13*, 3249. [[CrossRef](#)] [[PubMed](#)]
46. Luo, W.; Cheng, L.; Yuan, C.; Wu, Z.; Yuan, G.; Hou, M.; Chen, J.Y.; Luo, C.; Li, W. Preparation, characterization and evaluation of cellulose nanocrystal/poly(lactic acid) in situ nanocomposite scaffolds for tissue engineering. *Int. J. Biol. Macromol.* **2019**, *134*, 469–479. [[CrossRef](#)] [[PubMed](#)]

47. Sun, B.; Zhang, M.; Hou, Q.; Liu, R.; Wu, T.; Si, C. Further characterization of cellulose nanocrystal (CNC) preparation from sulfuric acid hydrolysis of cotton fibers. *Cellulose* **2016**, *23*, 439–450. [[CrossRef](#)]
48. Barbosa, A.M.; Robles, E.; Ribeiro, J.S.; Lund, R.G.; Carreño, N.L.V.; Labidi, J. Cellulose Nanocrystal Membranes as Excipients for Drug Delivery Systems. *Materials* **2016**, *9*, 1002. [[CrossRef](#)] [[PubMed](#)]
49. Kusmono; Listyanda, R.F.; Wildan, M.W.; Ilman, M.N. Preparation and characterization of cellulose nanocrystal extracted from ramie fibers by sulfuric acid hydrolysis. *Heliyon* **2020**, *6*, e05486. [[CrossRef](#)]
50. Xu, Y.; Atrens, A.D.; Stokes, J.R. Liquid crystal hydroglass formed via phase separation of nanocellulose colloidal rods. *Soft Matter* **2019**, *15*, 1716–1720. [[CrossRef](#)] [[PubMed](#)]
51. Thompson, L.; Azadmanjiri, J.; Nikzad, M.; Sbarski, I.; Wang, J.; Yu, A. Cellulose Nanocrystals: Production, Functionalization and Advanced Applications. *Rev. Adv. Mater. Sci.* **2019**, *58*, 1–16. [[CrossRef](#)]
52. Dufresne, A. Nanocellulose: A new ageless bionanomaterial. *Mater. Today* **2013**, *16*, 220–227. [[CrossRef](#)]
53. Chirayil, C.J.; Mathew, L.; Thomas, S. Review of recent research in nano cellulose preparation from different lignocellulosic fibers. *Rev. Adv. Mater. Sci.* **2014**, *37*, 20–28.
54. Ilyas, R.; Sapuan, S.; Atikah, M.; Asyraf, M.; Rafiqah, S.A.; Aisyah, H.; Nurazzi, N.M.; Norrrahim, M. Effect of hydrolysis time on the morphological, physical, chemical, and thermal behavior of sugar palm nanocrystalline cellulose (*Arenga pinnata* (Wurmb.) Merr). *Text. Res. J.* **2021**, *91*, 152–167. [[CrossRef](#)]
55. Ilyas, R.; Sapuan, S.; Ishak, M.; Zainudin, E. Sugar palm nanofibrillated cellulose (*Arenga pinnata* (Wurmb.) Merr): Effect of cycles on their yield, physic-chemical, morphological and thermal behavior. *Int. J. Biol. Macromol.* **2018**, *123*, 379–388. [[CrossRef](#)] [[PubMed](#)]
56. Roslan, Z.B.; Ramli, Z.; Razman, M.R.; Asyraf, M.R.M.; Ishak, M.R.; Ilyas, R.A.; Nurazzi, N.M. Reflections on Local Community Identity by Evaluating Heritage Sustainability Protection in Jugra, Selangor, Malaysia. *Sustainability* **2021**, *13*, 8705. [[CrossRef](#)]
57. Fareez, I.M.; Jasni, A.H.; Norrrahim, M.N.F. Nanofibrillated Cellulose Based Bio-phenolic Composites. In *Phenolic Polymers Based Composite Materials*; Jawaid, M., Asim, M., Eds.; Springer: Singapore, 2021; pp. 139–151. [[CrossRef](#)]
58. Nurazzi, N.M.; Shazleen, S.; Aisyah, H.A.; Asyraf, M.; Sabaruddin, F.; Mohidem, N.; Norrrahim, M.N.F.; Kamarudin, S.; Ilyas, R.A.; Ishak, M.; et al. Effect of silane treatments on mechanical performance of kenaf fibre reinforced polymer composites: A review. *Funct. Compos. Struct.* **2021**, *3*, 045003. [[CrossRef](#)]
59. Lagerwall, J.P.F.; Schütz, C.; Salajkova, M.; Noh, J.; Park, J.H.; Scalia, G.; Bergström, L. Cellulose nanocrystal-based materials: From liquid crystal self-assembly and glass formation to multifunctional thin films. *NPG Asia Mater.* **2014**, *6*, e80. [[CrossRef](#)]
60. Luzi, F.; Puglia, D.; Sarasini, F.; Tirillò, J.; Maffei, G.; Zuurro, A.; Lavecchia, R.; Kenny, J.M.; Torre, L. Valorization and extraction of cellulose nanocrystals from North African grass: *Ampelodesmos mauritanicus* (Diss). *Carbohydr. Polym.* **2019**, *209*, 328–337. [[CrossRef](#)]
61. Hubbe, M.A.; Rojas, O.; Lucia, L.A.; Sain, M. Cellulosic nanocomposites. A review. *BioResources* **2008**, *3*, 929–980. [[CrossRef](#)]
62. Rånby, B.G.; Banderet, A.; Sillén, L.G. Aqueous Colloidal Solutions of Cellulose Micelles. *Acta Chem. Scand.* **1949**, *3*, 649–650. [[CrossRef](#)]
63. Araki, J.; Kuga, S. Effect of Trace Electrolyte on Liquid Crystal Type of Cellulose Microcrystals. *Langmuir* **2001**, *17*, 4493–4496. [[CrossRef](#)]
64. Heux, L.; Chauve, G.; Bonini, C. Nonflocculating and Chiral-Nematic Self-ordering of Cellulose Microcrystals Suspensions in Nonpolar Solvents. *Langmuir* **2000**, *16*, 8210–8212. [[CrossRef](#)]
65. Beck-Candanedo, S.; Roman, M.; Gray, D.G. Effect of Reaction Conditions on the Properties and Behavior of Wood Cellulose Nanocrystal Suspensions. *Biomacromolecules* **2005**, *6*, 1048–1054. [[CrossRef](#)]
66. Kimura, F.; Kimura, T.; Tamura, M.; Hirai, A.; Ikuno, A.M.; Horii, F. Magnetic Alignment of the Chiral Nematic Phase of a Cellulose Microfibril Suspension. *Langmuir* **2005**, *21*, 2034–2037. [[CrossRef](#)] [[PubMed](#)]
67. Revol, J.-F. On the cross-sectional shape of cellulose crystallites in *Valonia ventricosa*. *Carbohydr. Polym.* **1982**, *2*, 123–134. [[CrossRef](#)]
68. De Aguiar, J.; Bondancia, T.; Claro, P.I.C.; Mattoso, L.H.C.; Farinas, C.S.; Marconcini, J.M. Enzymatic Deconstruction of Sugarcane Bagasse and Straw to Obtain Cellulose Nanomaterials. *ACS Sustain. Chem. Eng.* **2020**, *8*, 2287–2299. [[CrossRef](#)]
69. Squinca, P.; Bilatto, S.; Badino, A.C.; Farinas, C.S. Nanocellulose Production in Future Biorefineries: An Integrated Approach Using Tailor-Made Enzymes. *ACS Sustain. Chem. Eng.* **2020**, *8*, 2277–2286. [[CrossRef](#)]
70. Siqueira, G.A.; Dias, I.K.R.; Arantes, V. Exploring the action of endoglucanases on bleached eucalyptus kraft pulp as potential catalyst for isolation of cellulose nanocrystals. *Int. J. Biol. Macromol.* **2019**, *133*, 1249–1259. [[CrossRef](#)] [[PubMed](#)]
71. Camargo, L.A.; Pereira, S.C.; Correa, A.C.; Farinas, C.S.; Marconcini, J.M.; Mattoso, L.H.C. Feasibility of Manufacturing Cellulose Nanocrystals from the Solid Residues of Second-Generation Ethanol Production from Sugarcane Bagasse. *BioEnergy Res.* **2016**, *9*, 894–906. [[CrossRef](#)]
72. Cui, S.; Zhang, S.; Ge, S.; Xiong, L.; Sun, Q. Green preparation and characterization of size-controlled nanocrystalline cellulose via ultrasonic-assisted enzymatic hydrolysis. *Ind. Crops Prod.* **2016**, *83*, 346–352. [[CrossRef](#)]
73. Alonso-Lerma, B.; Barandiaran, L.; Ugarte, L.; Larraza, I.; Reifs, A.; Olmos-Juste, R.; Barrietabeña, N.; Amenabar, I.; Hillenbrand, R.; Eceiza, A.; et al. High performance crystalline nanocellulose using an ancestral endoglucanase. *Commun. Mater.* **2020**, *1*, 57. [[CrossRef](#)]
74. Edgar, C.D.; Gray, D.G. Induced Circular Dichroism of Chiral Nematic Cellulose Films. *Cellulose* **2001**, *8*, 5–12. [[CrossRef](#)]

75. Xu, Y.; Atrens, A.; Stokes, J.R. Structure and rheology of liquid crystal hydroglass formed in aqueous nanocrystalline cellulose suspensions. *J. Colloid Interface Sci.* **2019**, *555*, 702–713. [[CrossRef](#)]
76. Xu, Y.; Atrens, A.; Stokes, J.R. A review of nanocrystalline cellulose suspensions: Rheology, liquid crystal ordering and colloidal phase behaviour. *Adv. Colloid Interface Sci.* **2020**, *275*, 102076. [[CrossRef](#)] [[PubMed](#)]
77. Xu, Y.; Atrens, A.D.; Stokes, J.R. “Liquid, gel and soft glass” phase transitions and rheology of nanocrystalline cellulose suspensions as a function of concentration and salinity. *Soft Matter* **2018**, *14*, 1953–1963. [[CrossRef](#)] [[PubMed](#)]
78. Zaccarelli, E. Colloidal gels: Equilibrium and non-equilibrium routes. *J. Phys. Condens. Matter* **2007**, *19*, 323101. [[CrossRef](#)]
79. Drwenski, T.; Dussi, S.; Hermes, M.; Dijkstra, M.; van Roij, R. Phase diagrams of charged colloidal rods: Can a uniaxial charge distribution break chiral symmetry? *J. Chem. Phys.* **2016**, *144*, 094901. [[CrossRef](#)] [[PubMed](#)]
80. Dierking, I.; Neto, A.M.F. Novel Trends in Lyotropic Liquid Crystals. *Crystals* **2020**, *10*, 604. [[CrossRef](#)]
81. Tran, A.; Boott, C.E.; MacLachlan, M.J. Understanding the Self-Assembly of Cellulose Nanocrystals—Toward Chiral Photonic Materials. *Adv. Mater.* **2020**, *32*, e1905876. [[CrossRef](#)] [[PubMed](#)]
82. Wang, Z.; Yuan, Y.; Hu, J.; Yang, J.; Feng, F.; Yu, Y.; Liu, P.; Men, Y.; Zhang, J. Origin of vacuum-assisted chiral self-assembly of cellulose nanocrystals. *Carbohydr. Polym.* **2020**, *245*, 116459. [[CrossRef](#)] [[PubMed](#)]
83. Cherpak, V.; Korolovych, V.F.; Geryak, R.; Turiv, T.; Nepal, D.; Kelly, J.; Bunning, T.J.; Lavrentovich, O.D.; Heller, W.T.; Tsukruk, V.V. Robust Chiral Organization of Cellulose Nanocrystals in Capillary Confinement. *Nano Lett.* **2018**, *18*, 6770–6777. [[CrossRef](#)] [[PubMed](#)]
84. Putz, K.W.; Compton, O.C.; Segar, C.; An, Z.; Nguyen, S.T.; Brinson, L.C. Evolution of Order during Vacuum-Assisted Self-Assembly of Graphene Oxide Paper and Associated Polymer Nanocomposites. *ACS Nano* **2011**, *5*, 6601–6609. [[CrossRef](#)]
85. Dumanli, A.G.; van der Kooij, H.M.; Kamita, G.; Reisner, E.; Baumberg, J.J.; Steiner, U.; Vignolini, S. Digital Color in Cellulose Nanocrystal Films. *ACS Appl. Mater. Interfaces* **2014**, *6*, 12302–12306. [[CrossRef](#)]
86. Salas, C.; Nypelö, T.; Rodriguez-Abreu, C.; Carrillo, C.; Rojas, O. Nanocellulose properties and applications in colloids and interfaces. *Curr. Opin. Colloid Interface Sci.* **2014**, *19*, 383–396. [[CrossRef](#)]
87. Espinha, A.; Guidetti, G.; Serrano, M.C.; Frka-Petesic, B.; Dumanli, A.G.; Hamad, W.Y.; Blanco, Á.; López, C.; Vignolini, S. Shape Memory Cellulose-Based Photonic Reflectors. *ACS Appl. Mater. Interfaces* **2016**, *8*, 31935–31940. [[CrossRef](#)] [[PubMed](#)]
88. Xu, M.; Li, W.; Ma, C.; Yu, H.; Wu, Y.; Wang, Y.; Chen, Z.; Li, J.; Liu, S. Multifunctional chiral nematic cellulose nanocrystals/glycerol structural colored nanocomposites for intelligent responsive films, photonic inks and iridescent coatings. *J. Mater. Chem. C* **2018**, *6*, 5391–5400. [[CrossRef](#)]
89. Jativa, F.; Schütz, C.; Bergström, L.; Zhang, X.; Wicklein, B. Confined self-assembly of cellulose nanocrystals in a shrinking droplet. *Soft Matter* **2015**, *11*, 5374–5380. [[CrossRef](#)]
90. Yang, J.; Ye, D.Y. Liquid crystal of nanocellulose whiskers’ grafted with acrylamide. *Chin. Chem. Lett.* **2012**, *23*, 367–370. [[CrossRef](#)]
91. Wan, H.; Li, X.; Zhang, L.; Liu, P.; Jiang, Z.; Yu, Z.-Z. Rapidly Responsive and Flexible Chiral Nematic Cellulose Nanocrystal Composites as Multifunctional Rewritable Photonic Papers with Eco-Friendly Inks. *ACS Appl. Mater. Interfaces* **2018**, *10*, 5918–5925. [[CrossRef](#)]
92. Cheng, Q.; Chen, P.; Ye, D.; Wang, J.; Song, G.; Liu, J.; Chen, Z.; Chen, L.; Zhou, Q.; Chang, C.; et al. The conversion of nanocellulose into solvent-free nanoscale liquid crystals by attaching long side-arms for multi-responsive optical materials. *J. Mater. Chem. C* **2020**, *8*, 11022–11031. [[CrossRef](#)]
93. Mu, X.; Gray, D.G. Formation of Chiral Nematic Films from Cellulose Nanocrystal Suspensions Is a Two-Stage Process. *Langmuir* **2014**, *30*, 9256–9260. [[CrossRef](#)]
94. Kobayashi, Y.; Saito, A.P.T.; Isogai, A. Aerogels with 3D Ordered Nanofiber Skeletons of Liquid-Crystalline Nanocellulose Derivatives as Tough and Transparent Insulators. *Angew. Chem. Int. Ed.* **2014**, *53*, 10394–10397. [[CrossRef](#)]
95. Meng, X.; Pan, H.; Lu, T.; Chen, Z.; Chen, Y.; Zhang, D.; Zhu, S. Photonic-structured fibers assembled from cellulose nanocrystals with tunable polarized selective reflection. *Nanotechnology* **2018**, *29*, 325604. [[CrossRef](#)]
96. Saha, P.; Davis, V.A. Photonic Properties and Applications of Cellulose Nanocrystal Films with Planar Anchoring. *ACS Appl. Nano Mater.* **2018**, *1*, 2175–2183. [[CrossRef](#)]
97. Giese, M.; Blusch, L.K.; Khan, M.K.; Hamad, W.Y.; MacLachlan, M.J. Responsive Mesoporous Photonic Cellulose Films by Supramolecular Cotemplating. *Angew. Chem. Int. Ed.* **2014**, *53*, 8880–8884. [[CrossRef](#)] [[PubMed](#)]
98. Chu, G.; Qu, D.; Zussman, E.; Xu, Y. Ice-Assisted Assembly of Liquid Crystalline Cellulose Nanocrystals for Preparing Anisotropic Aerogels with Ordered Structures. *Chem. Mater.* **2017**, *29*, 3980–3988. [[CrossRef](#)]
99. Bardet, R.; Belgacem, N.; Bras, J. Flexibility and Color Monitoring of Cellulose Nanocrystal Iridescent Solid Films Using Anionic or Neutral Polymers. *ACS Appl. Mater. Interfaces* **2014**, *7*, 4010–4018. [[CrossRef](#)] [[PubMed](#)]
100. Parker, R.M.; Guidetti, G.; Williams, C.A.; Zhao, T.; Narkevicius, A.; Vignolini, S.; Frka-Petesic, B. The Self-Assembly of Cellulose Nanocrystals: Hierarchical Design of Visual Appearance. *Adv. Mater.* **2018**, *30*, e1704477. [[CrossRef](#)]
101. Guidetti, G.; Atifi, S.; Vignolini, S.; Hamad, W.Y. Flexible Photonic Cellulose Nanocrystal Films. *Adv. Mater.* **2016**, *28*, 10042–10047. [[CrossRef](#)]
102. Yao, K.; Meng, Q.; Bulone, V.; Zhou, Q. Flexible and Responsive Chiral Nematic Cellulose Nanocrystal/Poly(ethylene glycol) Composite Films with Uniform and Tunable Structural Color. *Adv. Mater.* **2017**, *29*, 1701323. [[CrossRef](#)]
103. Cheung, C.C.Y.; Giese, M.; Kelly, J.A.; Hamad, W.Y.; MacLachlan, M.J. Iridescent Chiral Nematic Cellulose Nanocrystal/Polymer Composites Assembled in Organic Solvents. *ACS Macro Lett.* **2013**, *2*, 1016–1020. [[CrossRef](#)]

104. Shopsowitz, K.E.; Qi, H.; Hamad, W.Y.; MacLachlan, M. Free-standing mesoporous silica films with tunable chiral nematic structures. *Nature* **2010**, *468*, 422–425. [[CrossRef](#)]
105. Ureña-Benavides, E.E.; Kitchens, C.L. Cellulose Nanocrystal Reinforced Alginate Fibers—Biomimicry Meets Polymer Processing. *Mol. Cryst. Liq. Cryst.* **2012**, *556*, 275–287. [[CrossRef](#)]
106. He, Y.-D.; Zhang, Z.-L.; Xue, J.; Wang, X.-H.; Song, F.; Wang, X.-L.; Zhu, L.-L.; Wang, Y.-Z. Biomimetic Optical Cellulose Nanocrystal Films with Controllable Iridescent Color and Environmental Stimuli-Responsive Chromism. *ACS Appl. Mater. Interfaces* **2018**, *10*, 5805–5811. [[CrossRef](#)] [[PubMed](#)]
107. Frka-Petesic, B.; Radavidson, H.; Jean, B.; Heux, L. Dynamically Controlled Iridescence of Cholesteric Cellulose Nanocrystal Suspensions Using Electric Fields. *Adv. Mater.* **2017**, *29*, 1606208. [[CrossRef](#)] [[PubMed](#)]
108. Fernandes, S.N.; Almeida, P.L.; Monge, N.; Aguirre, L.E.; Reis, D.; de Oliveira, C.L.P.; Neto, A.M.F.; Pieranski, P.; Godinho, M.H. Mind the Microgap in Iridescent Cellulose Nanocrystal Films. *Adv. Mater.* **2016**, *29*, 1603560. [[CrossRef](#)] [[PubMed](#)]
109. Chen, Q.; Liu, P.; Nan, F.; Zhou, L.; Zhang, J. Tuning the Iridescence of Chiral Nematic Cellulose Nanocrystal Films with a Vacuum-Assisted Self-Assembly Technique. *Biomacromolecules* **2014**, *15*, 4343–4350. [[CrossRef](#)]
110. Bruel, C.; Tavares, J.R.; Carreau, P.J.; Heuzey, M. Impact of colloidal stability on cellulose nanocrystals self-ordering in thin films. *TechConnect Briefs* **2019**, *2019*, 61–64.
111. Beck, S.; Bouchard, J.; Berry, R. Controlling the Reflection Wavelength of Iridescent Solid Films of Nanocrystalline Cellulose. *Biomacromolecules* **2011**, *12*, 167–172. [[CrossRef](#)]
112. Walters, C.M.; Boott, C.E.; Nguyen, T.-D.; Hamad, W.Y.; MacLachlan, M.J. Iridescent Cellulose Nanocrystal Films Modified with Hydroxypropyl Cellulose. *Biomacromolecules* **2020**, *21*, 1295–1302. [[CrossRef](#)]
113. Zhu, H.; Fang, Z.; Wang, Z.; Dai, J.; Yao, Y.; Shen, F.; Preston, C.; Wu, W.; Peng, P.; Jang, N.; et al. Extreme Light Management in Mesoporous Wood Cellulose Paper for Optoelectronics. *ACS Nano* **2016**, *10*, 1369–1377. [[CrossRef](#)]
114. Chindawong, C.; Johannsmann, D. An anisotropic ink based on crystalline nanocellulose: Potential applications in security printing. *J. Appl. Polym. Sci.* **2014**, *131*, 41063. [[CrossRef](#)]
115. Bar-On, B.; Sui, X.; Livanov, K.; Achrai, B.; Kalfon-Cohen, E.; Wiesel, E.; Wagner, H.D. Structural origins of morphing in plant tissues. *Appl. Phys. Lett.* **2014**, *105*, 033703. [[CrossRef](#)]
116. Wu, T.; Li, J.; Li, J.; Ye, S.; Wei, J.; Guo, J. A bio-inspired cellulose nanocrystal-based nanocomposite photonic film with hyper-reflection and humidity-responsive actuator properties. *J. Mater. Chem. C* **2016**, *4*, 9687–9696. [[CrossRef](#)]
117. Raviv, R.; Zhao, W.; Mcknelly, C.L.; Papadopoulou, A.; Kadambi, A.; Shi, B.; Hirsch, S.; Dikovsky, D.; Zyracki, M.; Olguin, C.; et al. Active Printed Materials for Complex Self-Evolving Deformations. *Sci. Rep.* **2014**, *4*, 7422. [[CrossRef](#)] [[PubMed](#)]
118. Siqueira, G.; Kokkinis, D.; Libanori, R.; Hausmann, M.K.; Gladman, A.S.; Neels, A.; Tingaut, P.; Zimmermann, T.; Lewis, J.A.; Studart, A.R. Cellulose Nanocrystal Inks for 3D Printing of Textured Cellular Architectures. *Adv. Funct. Mater.* **2017**, *27*, 1604619. [[CrossRef](#)]
119. Shahzadi, K.; Mohsin, I.; Wu, L.; Ge, X.; Jiang, Y.; Li, H.; Mu, X. Bio-Based Artificial Nacre with Excellent Mechanical and Barrier Properties Realized by a Facile In Situ Reduction and Cross-Linking Reaction. *ACS Nano* **2017**, *11*, 325–334. [[CrossRef](#)]
120. Bobbert, F.S.L.; Zadpoor, A.A. Effects of bone substitute architecture and surface properties on cell response, angiogenesis, and structure of new bone. *J. Mater. Chem. B* **2017**, *5*, 6175–6192. [[CrossRef](#)]
121. Huang, C.; Bhagia, S.; Hao, N.; Meng, X.; Liang, L.; Yong, Q.; Ragauskas, A.J. Biomimetic composite scaffold from an in situ hydroxyapatite coating on cellulose nanocrystals. *RSC Adv.* **2019**, *9*, 5786–5793. [[CrossRef](#)]
122. Fernandes, S.N.; Geng, Y.; Vignolini, S.; Glover, B.J.; Trindade, A.C.; Canejo, J.P.; Almeida, P.L.; Brogueira, P.; Godinho, M.H. Structural Color and Iridescence in Transparent Sheared Cellulosic Films. *Macromol. Chem. Phys.* **2013**, *214*, 25–32. [[CrossRef](#)]